JGR Atmospheres

RESEARCH ARTICLE
10.1029/2024JD041965

Stratus and Stratocumulus Cloud Microphysics and Drizzle Relationships With CCN Modality

James G. Hudson[1] and Stephen Noble[2]

[1]Desert Research Institute, Reno, NV, USA, [2]Savannah River National Laboratory, Aiken, SC, USA

Key Points:

- In two stratus cloud projects bimodal cloud condensation nuclei (CCN) spectra are associated with clouds that have more droplets with smaller sizes and less drizzle
- However, in cleaner Physics of Stratocumulus Tops stratus clouds bimodal CCN spectra are associated with fewer but larger droplets yet also less drizzle
- These findings suggest that cloud processing of aerosol could enhance the indirect aerosol effect (IAE) in stratus, especially 2nd IAE

Supporting Information:

Supporting Information may be found in the online version of this article.

Correspondence to:

J. G. Hudson,
hudson@dri.edu

Citation:

Hudson, J. G., & Noble, S. (2024). Stratus and stratocumulus cloud microphysics and drizzle relationships with CCN modality. *Journal of Geophysical Research: Atmospheres*, *129*, e2024JD041965. https://doi.org/10.1029/2024JD041965

Received 10 JUL 2024
Accepted 21 OCT 2024

Author Contributions:

Conceptualization: James G. Hudson
Data curation: James G. Hudson
Formal analysis: James G. Hudson
Funding acquisition: James G. Hudson
Investigation: James G. Hudson
Methodology: James G. Hudson
Project administration: James G. Hudson
Resources: James G. Hudson
Software: Stephen Noble
Supervision: James G. Hudson
Validation: James G. Hudson, Stephen Noble
Writing – original draft: James G. Hudson
Writing – review & editing: James G. Hudson, Stephen Noble

Abstract High resolution extended-range cloud condensation nuclei (CCN) spectral comparisons with cloud microphysics and drizzle of the Physics of Stratocumulus Tops (POST) field experiment confirmed results in the Marine Stratus/Stratocumulus Experiment (MASE). Both of these stratus cloud projects demonstrated that bimodal CCN spectra typically caused by cloud processing were associated with clouds that exhibited higher concentrations of smaller droplets with narrower distributions and less drizzle than clouds associated with unimodal CCN spectra. Resulting brighter clouds and increased cloudiness could enhance both indirect aerosol effects (IAE). These stratus findings are opposite of analogous measurements in two cumulus cloud projects, which showed bimodal CCN associated with fewer larger droplets more broadly distributed and with more drizzle than clouds associated with unimodal CCN. Resulting reduced cumulus brightness and cloudiness could reduce both IAE. Physics of Stratocumulus Tops (POST) flights in air masses with higher CCN concentrations, N_{CCN}, showed more extremes of the stratus characteristics. However, POST flights with lower N_{CCN} showed opposite droplet characteristics similar to the cumulus clouds, yet still showed less drizzle in clouds associated with bimodal CCN, but not as much less as the flights with higher N_{CCN}. Since all MASE clouds were in polluted air masses, while the two cumulus projects were in clean air masses we deduce from these four projects that both the dynamic stratus/cumulus differences (vertical wind) and N_{CCN} are responsible for the microphysics and drizzle differences among these projects. This is because the clean POST characteristics are a hybrid between MASE/POST high N_{CCN} and the two cumulus projects.

Plain Language Summary The Physics of Stratocumulus Tops (POST) project displayed relationships between the particles that cloud droplets condense upon (cloud condensation nuclei; CCN) and cloud and drizzle drop concentrations that are consistent with those in the Marine Stratus/Stratocumulus Experiment (MASE). CCN spectra composed of two separate modes that are often caused by chemical and physical process mechanisms within the clouds were associated with clouds that had greater concentrations of smaller droplets and less drizzle than clouds associated with single mode (unimodal) CCN spectra. These findings are opposite of analogous analyses of two cumulus cloud projects. However, a subset of POST clouds in cleaner air showed bimodal CCN associated with clouds that had fewer but larger droplets yet still less drizzle than clouds associated with unimodal CCN. These clean stratus results are thus similar to the cumulus findings with respect to cloud droplets but opposite of the cumulus drizzle findings. Therefore, throughout POST bimodal CCN were associated with clouds that contained less drizzle than clouds associated with unimodal CCN. However, the apparent bimodal CCN drizzle suppression was less in the cleaner POST clouds.

1. Introduction

The indirect aerosol effect (IAE), the largest climate uncertainty (Christensen et al., 2020; Douglas & L'Ecuyer, 2020; Intergovernmental Panel on Climate Change, 2021; Masson-Delmotte et al., 2021; Mulmenstadt & Feingold, 2018) is mostly due to more cloud condensation nuclei (CCN) causing higher cloud droplet concentrations, N_c, in low altitude maritime stratus (Kogan et al., 1996; Warren et al., 1988). These clouds are climatically important because their high radiative temperature cooling effect provides large albedo contrasts with the exposed ocean. Higher CCN concentrations, N_{CCN}, due to air pollution, enhance marine stratus cloud cooling. Greater droplet surface areas of higher N_c is cloud brightening 1st IAE (Twomey, 1977). Consequent smaller cloud droplets that inhibit drizzle formation can spatially and temporally enhance cloudiness. This 2nd IAE cloud lifetime effect (Albrecht, 1989) increase of planetary albedo is further global cooling. Rosenfeld et al. (2019), Wall et al. (2023), and Christensen et al. (2024) have expanded 2nd IAE because drizzle suppression tends to increase cloud fraction. Low N_{CCN} and low N_c characteristic of maritime air make these clouds even more susceptible to pollution influences (Gryspeerdt et al., 2023; Platnick & Twomey, 1994).

Table 1
Projects Being Compared to Physics of Stratocumulus Tops

Acronym	Name	Time	Clouds	Location	Concentration	Citation	Abbreviation
MASE	Marine Stratus/Stratocumulus Experiment	July, 2005	Warm low stratus	Off central California coast.	Polluted	Hudson et al. (2018)	H18
ICE-T	Ice in Clouds-Tropical	July–August, 2011	Low altitude warm cumuli	Eastern Caribbean	Clean maritime	Hudson and Noble (2020)	HN20
RICO	Rain in Cumulus over the Ocean	December–January, 2003-2004	Low altitude warm cumuli	Eastern Caribbean	Clean maritime	Hudson and Noble (2022)	HN22
POST	Physics of Stratocumulus Tops	July–August, 2008	Warm low stratus	Off central California coast.	Polluted and clean	Current study	

When Hoppel et al. (1985, 1986, 1990, 1994, 1996; hereafter H85-96) found bimodal aerosol size distributions only where there were clouds they demonstrated that gas-to-particle chemical reactions within droplets (O'Dowd et al., 1999; Yang et al., 2011) and cloud droplet Brownian capture of interstitial material (Svenningsson et al., 1997) could be the only cause. Feingold et al. (1996) added coalescence among droplets, which also converts some smaller Aitken mode particles that nucleated cloud droplets to larger accumulation mode particles, after the droplets evaporate as they usually do. These three processes make aerosol and CCN bimodality. Other possible sources of accumulation mode particles cannot produce the minimum concentrations between modes that are characteristic of bimodal aerosol/CCN (H85-96). Clarke et al. (1996, 1998, 1999, 2004, 2013; hereafter C96-13), Hoffmann (1993), Garrett and Hobbs (1995), Van Dingenen et al. (1995), Jensen et al. (1996), Covert et al. (1996), Weber et al. (1997), Weingartner et al. (1999), Birmili et al. (2001), Tunved et al. (2003), Tomlinson et al. (2007), Kleinman et al. (2012), Shingler et al. (2012), Modini et al. (2015) and others have confirmed the bimodal aerosol association with cloudiness.

In the Marine Stratus/Stratocumulus Experiment (MASE), clouds associated with bimodal high-resolution differential CCN spectra over an extended range of supersaturations (S) had greater N_c, with smaller mean diameters, MD, smaller standard deviations, sd, of droplet spectra, σ, and less drizzle (Hudson et al., 2018; hereafter H18). But analogous measurements in low altitude warm cumuli of the Ice in Clouds-Tropical (ICE-T) experiment (Hudson & Noble, 2020; hereafter HN20) showed that bimodal CCN spectra were associated with clouds that had lower N_c, larger MD and σ and greater drizzle than clouds associated with unimodal CCN spectra. Analysis of another cumulus project, Rain in Cumulus over the Ocean, (RICO), by Hudson and Noble (2022; hereafter HN22) then confirmed the ICE-T findings. Table 1 lists the three previous projects that POST is compared to along with the associated citations and abbreviations.

Noble and Hudson (2019; hereafter NH19) demonstrated that clouds caused the accumulation mode that characterizes bimodal aerosol in north central Oklahoma. This conclusion was mainly due to the stability of accumulation mode concentrations and decreased accumulation mode size during consecutive cloudless hours and increased accumulation mode concentration and size during consecutive cloudy hours. Close relationships of subcloud CCN modality with low altitude RICO cloudiness but not with low altitude N_c support cloud processing effects on CCN whereas RICO clouds that were too high to influence low altitude CCN showed only the effect of CCN on N_c (Hudson & Noble, 2021).

We now examine the Physics of Stratocumulus Tops (POST) project (Carman et al., 2012; Gerber et al., 2013; Hudson et al., 2010, hereafter H10; Hudson & Noble, 2014a, 2014b), to determine how another set of stratus clouds compares to the H18 MASE observations. H18 indicated that greater droplet concentrations and less drizzle associated with bimodal CCN in MASE may have respectively enhanced 1st and 2nd IAE. However, the lower droplet concentrations and greater drizzle in clouds associated with bimodal CCN seemed to reduce both IAE in ICE-T (HN20) and RICO (HN22). Because of the same research project and the common topic of CCN and clouds much of this and the next section were also presented in H10 and Hudson and Noble (2014a, 2014b).

2. Measurements

POST occurred in July–August 2008 off the central California coast where all measurements were made on board the CIRPAS Twin Otter airplane based at Marina, California. CCN were measured by a Desert Research Institute

CCN spectrometer (Hudson, 1989) that was calibrated more than once during each flight. Presented N_{CCN} are simultaneous averages over the 0.02%–1.5% S range during horizontal flight legs below the clouds. Cloud droplets were measured with a Cloud Aerosol Spectrometer (CAS) probe (diameter 0.58–51 μm). The presented N_c are average concentrations of droplets larger than 0.58 μm diameter (dia) for those one second periods when CAS liquid water content (LWC) exceeded 0.10 or 0.35 g/m^3. Drizzle was measured by the cloud imaging probe (CAP) for drops between 50 and 1,500 μm dia. CAS and CAP are components of the cloud, aerosol and precipitation spectrometer of Droplet Measurements Technologies of Boulder, Colorado (Baumgardner, 1983). Vertical wind, W, was measured with a GPS corrected C-MIGITS III using the technique of Lenschow and Spyers-Duran (1989).

In MASE, ICE-T, RICO and now POST CCN modality is characterized by the normalized N_{CCN} differences, ndf, between the two CCN modes, N_p, the ostensibly cloud processed larger dia (lower S) accumulation mode, and N_u, the unprocessed smaller dia (higher S) Aitken mode. Thus, ndf = $(N_p - N_u)/(N_p + N_u)$, characterizes the entire CCN spectrum. Lower ndf indicates more bimodal CCN spectra and higher ndf indicates more unimodal CCN spectra. Bimodal CCN in POST showed distinct S minima (Hoppel minima) between the two modes (Figure S1 in Supporting Information S1). Table S1 in Supporting Information S1 shows the various means and sd of the measured CCN spectra pertinent to the figures and tables that are presented.

As in MASE, ICE-T, RICO and POST clouds consisted of all 1s microphysics measurements within each constant-altitude horizontal flight leg that encountered cloud droplet LWC, L_c, greater than 0.10 or 0.35 g/m^3. All cloud parcels within each constant-altitude horizontal flight leg that met these L_c thresholds are considered together as a single *cloud* and are denoted as such by italicized print. Depending on the L_c threshold used to define clouds, the cloud parcels that met these criteria are sometimes separated by non-cloud parcels between some cloud parcels within the same horizontal flight leg.

Clouds in H18, H20, H22 and here in POST are then classified according to ndf of the below cloud CCN spectrum closest to each *cloud*. All *clouds* and thus all microphysics measurements are then divided into six groups according to higher and lower ndf halves, highest and lowest ndf quartiles and highest and lowest ndf octiles. The greater numbers of *clouds* than CCN measurements means that some *cloud* multiples are associated with the same CCN spectrum. This sometimes results in disproportionate numbers of *clouds* within some of the six groups as documented in figure legends. All POST data considered here are available at NCAR-RAF (2022).

3. Results

Figures 1a–1d demonstrates that POST cloud droplet spectral relationships with CCN modality resemble MASE H18 Figure 4. This is because the black circle, blue square and cyan triangle (darker colors) droplet spectra associated, respectively, with lowest ndf octile, lowest ndf quartile and lower ndf half bimodal CCN spectra display higher peak concentrations than red octagon, orange diamond and pink inverted triangle (lighter colors) droplet spectra that are, respectively, associated with highest ndf octile, highest ndf quartile and higher ndf half unimodal CCN spectra in Figures 1a and 1b. Droplet concentrations are greater in *clouds* associated with bimodal CCN because of the abundance of CCN active at the low S characteristic of stratus due to limited W. Lack of low S CCN in unimodal-CCN-associated *clouds* produce lower droplet concentrations that can thus grow to larger sizes as is apparent with the secondary larger distributions where there are more larger droplets in unimodal-CCN associated *clouds*. The three higher bimodal peaks are even in modality order (black, blue and then cyan). As in MASE the 3 unimodal lines (lighter colors) cross the 3 bimodal lines so that Figures 1c and 1d show the 3 sets of *clouds* associated with unimodal CCN spectra with greater large cloud droplet mean concentrations than means of the 3 sets of *clouds* associated with bimodal CCN as was exhibited in H18 Figure 4c. This transition occurs because of the basic cloud physics principle that greater small droplet concentrations limit concentrations of larger cloud droplets. Figures 1c and 1d relative patterns continue into the Figures 1e and 1f drizzle size range where *clouds* associated with unimodal CCN (lighter colors) display more drizzle than *clouds* associated with bimodal CCN (darker colors). This same relative difference was displayed in Figure 5 of H18 where drizzle amounts were also in CCN modality order from highest octile (red), highest quartile (orange), higher half (pink), lower half (cyan), lowest quartile (blue) to lowest octile (black). This same modality order occurs between 300 and 450 μm in Figure 1e.

Analogous to Table 1 of H18, Table 2 now summarizes Figure 1 and other cloud measurements. Mean values of MD, σ, L_c, total drizzle drop concentration, N_d, and total drizzle drop LWC, L_d, are all greater in *clouds* associated

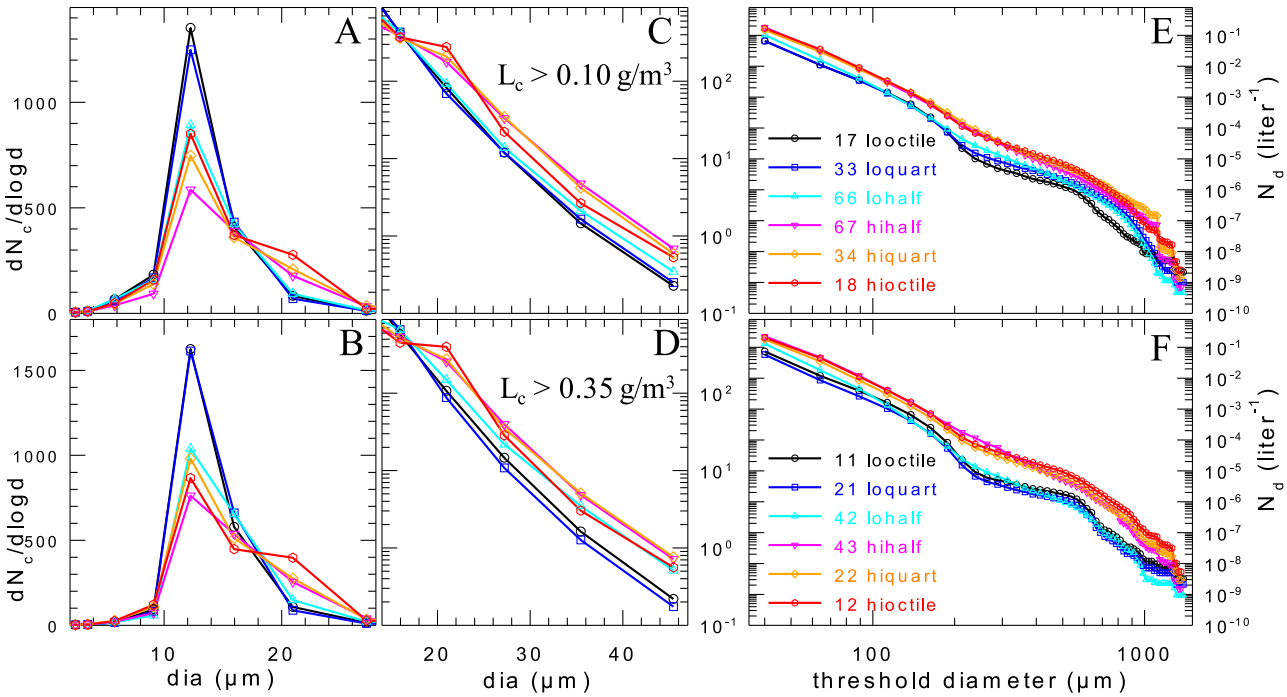

Figure 1. All 141 *clouds* with 54 cloud condensation nuclei (CCN) spectra of all 14 physics of stratocumulus tops flights. (a–d) Are differential cloud droplet spectra; (e, f) are cumulative drizzle drop spectra. Droplet and drop spectra are put into 6 groups according to ndf as noted in panels (e, f) legends, which also apply to the two panels directly left. (a, c, e) use $L_c > 0.1$ g/m^3 threshold with only 133 *clouds* but still 54 CCN spectra. (b, d, f) use $L_c > 0.35$ g/m^3 threshold with only 85 *clouds* and 44 CCN spectra. Ordinate labels to the right of (c, d) pertain only to (c, d). Height bias corrected.

with more unimodal CCN (high ndf) than *clouds* associated with more bimodal CCN (low ndf). This is so for both POST L_c thresholds and MASE (H18). Greater means and sd for adjacent-paired columns for halves, quartiles and octiles in each row are denoted by bold print. Therefore, the 3 higher ndf columns of H18 Tables 1 and 2 for mean MD, σ, L_c, N_d and L_d rows are bold. And as also displayed for MASE, mean N_c are greater in *clouds* associated with bimodal CCN (lower ndf). This is due to inherently greater low S N_{CCN} of bimodal distributions and the limited cloud S because of lower W characteristic of stratus. Complementary smaller MD and σ follow the higher N_c associated with bimodal CCN, which also tend to inhibit drizzle compared to lower N_c and larger MD and σ in clouds associated with unimodal CCN, which enhance collision-coalescence.

POST mean L_c are significantly greater than MASE mean L_c, none of which exceeded 0.18 g/m^3. This is due to the thicker POST clouds, which also account for greater mean MD and probably greater mean drizzle than MASE. All 6 MASE mean MD are less than 10 μm and all 6 MASE mean N_d are less than 7 cm^{-3} while all 6 MASE mean L_d are less than 4 mg/m^3. In spite of the ∼50% larger POST mean MD for some $L_c > 0.10$ g/m^3 columns, mean σ are remarkably similar between the two projects. This relative difference between MD and σ between projects is consistent with adiabatic predictions that σ decreases as droplets grow. Furthermore, larger mean MD for $L_c > 0.35$ g/m^3 are accompanied by smaller mean σ than for 0.10 g/m^3 L_c threshold. Narrower droplet spectra at larger MD suggest that POST microphysics is not greatly perturbed from adiabatic characteristics by entrainment or mixing.

3.1. Height Bias

Since many Table 2 parameters are known to be functions of distance above cloud base, height, the greater mean heights in the three higher ndf columns indicate that the differences noted above can also be due to height differences among the cloud measurements. This is especially so for L_c and MD, which definitely increase with height in adiabatic clouds and are consistently greater in the higher ndf columns. Height differences were also present in H18 Table 1 but since those greater mean heights were in lower ndf columns, the observed microphysics differences should have only been reduced from what they might have been had the mean heights been equal. But since the height and ndf differences in POST Table 2 seem to push in the same direction, microphysics

Table 2

Mean and Standard Deviation of ndf, Droplet Concentration (N_c, cm^{-3}), Droplet Mean Diameter (MD, μm), Droplet Spectral Width (σ, μm), Droplet Liquid Water Content (LWC) (L_c, g/m^3), Drizzle Drop Concentration (N_d, L^{-1}), Drizzle LWC (L_d, mg/m^3), Vertical Wind Standard Deviation (σ_w, m/s), and Distance Above Cloud Base, Height (Hgt, m), for All 14 Physics of Stratocumulus Tops Flights for $L_c > 0.10$ and > 0.35 g/m^3

		Low half		High half		Low quartile		High quartile		Low octile		High octile	
$L_c > 0.10$	ndf	0.057	**±0.192**	**0.525**	±0.178	−0.100	**±0.147**	**0.677**	±0.106	−0.200	**±0.129**	**0.758**	±0.081
	N_c	**216**	±86	166	**±87**	**250**	±87	192	**±93**	**267**	±88	209	**±94**
	MD	12.94	±2.77	**14.55**	**±3.44**	12.66	±2.33	**14.31**	**±3.64**	12.70	±2.71	**14.45**	**±3.61**
	σ	4.10	±1.30	**4.92**	**±1.47**	3.71	±1.24	**4.57**	**±1.42**	3.51	**±1.09**	**3.97**	±0.58
	L_c	0.282	±0.095	**0.302**	**±0.112**	0.304	±0.095	**0.328**	**±0.124**	0.319	±0.094	**0.357**	**±0.134**
	N_d	95	±116	**190**	**±131**	57	±80	**155**	**±114**	53	±81	**181**	**±115**
	L_d	12	±16	**25**	**±19**	7.9	±13	**23**	**±18**	7.3	±15	**26**	**±19**
	σ_w	0.491	**±0.137**	**0.496**	±0.134	**0.520**	**±0.137**	0.517	±0.111	**0.510**	**±0.107**	0.509	±0.099
	hgt	170	**±87**	**200**	±83	179	**±107**	**212**	±101	181	**±115**	**236**	±76
$L_c > 0.35$	ndf	0.044	**±0.214**	**0.559**	±0.189	−0.129	**±0.163**	**0.725**	±0.100	−0.207	**±0.143**	**0.812**	±0.035
	N_c	**231**	±97	204	**±98**	**287**	±91	224	**±112**	**284**	±99	237	**±126**
	MD	14.63	±2.19	**15.68**	**±3.30**	13.74	±1.73	**15.58**	**±3.47**	13.80	±2.00	**15.76**	**±3.61**
	σ	3.86	**±1.48**	**4.30**	±1.15	3.05	±1.09	**4.19**	**±1.18**	3.20	**±1.28**	**3.64**	±0.48
	L_c	0.402	±0.032	**0.424**	**±0.057**	0.412	±0.034	**0.448**	**±0.070**	0.409	±0.038	**0.467**	**±0.079**
	N_d	119	±158	**228**	**±281**	45	±69	**197**	**±135**	53	±81	**182**	**±89**
	L_d	14	±20	**32**	**±47**	5.8	±12	**27**	**±19**	7.3	±15	**27**	**±15**
	σ_w	0.473	**±0.233**	**0.511**	±0.144	0.527	**±0.193**	**0.535**	±0.113	0.473	**±0.184**	**0.547**	±0.100
	hgt	217	±54	**223**	**±76**	231	±66	**251**	**±75**	226	±73	**247**	**±76**

Note. Higher mean values of each parameter for halves, quartiles and octiles are denoted with bold print. Not height-bias corrected.

ndf attribution is problematic. The remedy discussed in H18 uses linear regressions of plots of each measured variable against height. These regression equations are solved at each mean height so that half of the fractions between these calculated differences and the mean measured differences can be subtracted or added as appropriate to each measured mean to estimate mean values beyond that attributable to mean height differences. Table 3 presents the ratios of these adjusted means in the high ndf columns to these adjusted means in the adjacent-pair low ndf columns. Thus, ratios greater than 1 indicate CCN unimodality dominance while ratios less than 1 indicate CCN bimodality dominance.

For all 14 POST flights for $L_c > 0.1$ g/m^3 the MD and L_c linear regressions with height are positive with correlation coefficients, R, of 0.62 and 0.66 and two-tailed probabilities, P2, less than 10^{-8}, which is as low as can be calculated. For the MD regression equation with height (Figure S2 in Supporting Information S1) the 9.44 m zero height intercept and the 0.023 μm/m slope when solved at the mean measured heights of 170 and 200 m of the low and high halves in Table 2 for $L_c > 0.10$ g/m^3 yield a height-bias of 13.398 μm at the low half and 14.096 μm at the high half. Half of this 0.698 μm MD height bias, 0.349 μm, is then added to the 12.94 μm measured MD mean at the 170 m mean height and 0.349 μm is subtracted from the 14.55 μm measured MD mean at the 200 m mean height to obtain 13.289 and 14.201 μm MD estimates. These are the MD that exceed the height bias. These height-biased-corrected mean MD estimates are divided to produce the 1.069 MD ratio denoted in the 3rd row 1st column of Table 3. Analogous regressions for each variable with height produce the POST ratios displayed in Table 3.

L_c and MD are the most obvious corrections because their relationships with height are the best understood, most frequently observed and acceptable to most atmospheric scientists. However, the essential variables for this analysis, N_c and N_d, display greater variabilities with height that are not as well established or understood. Therefore, regressions of these and other parameters with height have lower R and wider slope variations. Therefore, these height corrections are smaller than MD and L_c height corrections. For the 14 POST flights for $L_c > 0.1$ g/m^3 R for N_c and N_d with height are 0.26 and 0.35 with P2 of 0.002 and 0.0009. Some height corrections in subsequent tables are substantial but most height-bias corrections to the figures, which are based on N_c and N_d,

Table 3
Ratios of Parameter Values Associated With High to Low ndf Halves, Quartiles and Octiles

	POST					
	$L_c > 0.10$ g/m^3			$L_c > 0.35$ g/m^3		
	hi/lo half	hi/lo quart	hi/lo octile	hi/lo half	hi/lo quart	hi/lo octile
ndf	0.468	0.766	0.958	0.515	0.854	1.019
N_c	0.803	0.801	0.835	0.895	0.812	0.869
MD	1.069	1.068	1.035	1.063	1.101	1.107
σ	1.162	1.186	1.055	1.107	1.341	1.108
L_c	0.986	0.992	0.982	1.049	1.067	1.120
N_d	1.794	2.269	2.539	1.875	3.774	2.985
L_d	1.891	2.511	2.788	2.214	3.797	3.088
σ_w	0.994	0.977	0.969	1.080	1.013	1.154
hgt	1.174	1.188	1.301	1.027	1.088	1.094
MASE						
ndf	0.550	0.850	1.060			
N_c	0.863	0.799	0.761			
MD	1.085	1.112	1.144			
σ	1.125	1.214	1.286			
L_c	1.111	1.225	1.241			
N_d	2.004	3.040	4.116			
L_d	2.187	3.380	5.065			
σ_w	0.933	0.867	0.813			
hgt	0.797	0.831	1.000			

Note. For all 14 POST flights for $L_c > 0.10$ g/m^3 and $L_c > 0.35$ g/m^3, MASE $L_c > 0.10$ g/m^3 (from Table 1 of H18). Ndf shows the difference instead of ratio. Height bias corrected for POST.

are difficult to discern as can be seen by comparing corresponding uncorrected Figures S3–S8 in Supporting Information S1.

Table 3 similarities between the two projects and between the two POST L_c thresholds are that all mean N_c are greater in bimodal-CCN-associated *clouds* (ratio <1) whereas all mean MD, σ, N_d, and L_d are greater in unimodal-CCN-associated *clouds* (ratio >1). The N_c/MD opposite complementary ratios result from the basic cloud physics principle that higher/lower small droplet concentrations lead to lower/higher large droplet concentrations. The largest unimodal biases in both projects and both POST L_c are for drizzle, N_d and L_d. The biggest Table 3 difference is the smaller POST drizzle ratios than corresponding MASE drizzle ratios: thus, greater unimodal-biased drizzle in MASE.

3.2. POST Differences

The 4–5 hr POST research flights started at two distinct hours, 1000 local Pacific Daylight Time (PDT) and 1600 PDT. These flight groups are referred to as day and night. Figure 2 shows significantly greater mean N_{CCN} at all S for the 8 night flights than the 6-day flights. This apparently caused the 50% greater night flight mean N_c in Table 4. The night flights show complementary smaller mean MD and mean σ than the day flights. The greater mean L_c of the night flights that is contrary to the smaller night mean heights may be due to less nighttime drizzle that could increase cloud lifetime (2nd IAE). These night/day differences are seemingly related to the lower night mean ndf, greater CCN bimodality.

Figure 3 for the 8 night flights is similar to Figure 1. Figures 3a and 3b demonstrate higher peak N_c than Figures 1a and 1b, especially for bimodals (darker) due to higher night N_{CCN}, especially at lower S because of more limited stratus cloud S due to lower W. Consequently Figures 3c and 3d demonstrate lower concentrations of large cloud

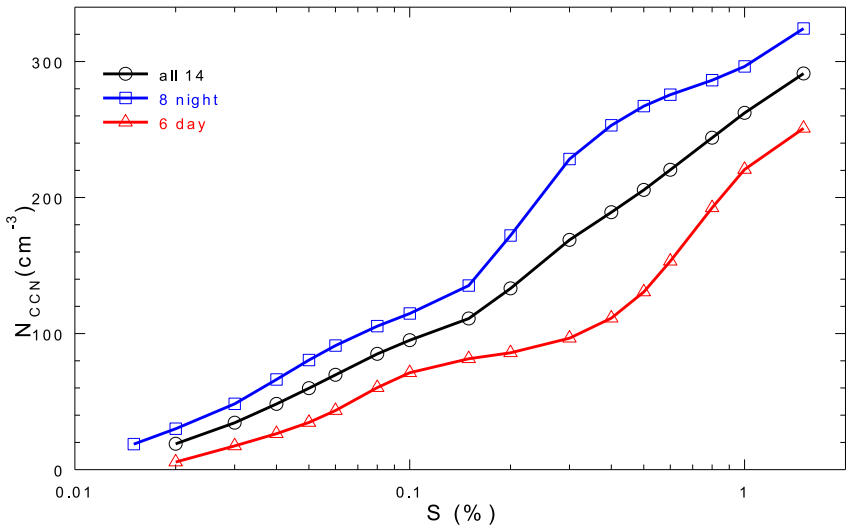

Figure 2. Mean composite cumulative cloud condensation nuclei (CCN) spectrum for the three flight categories. The number of supersaturation (S) channels is only 11 in order to compute these mean concentrations of the many CCN spectra involved for spectra applied to clouds with $L_c > 0.10$ g/m^3.

droplets than Figures 1c and 1d, especially for bimodal-CCN-associated *clouds* (darker colors). This is again because of the basic cloud physics principle that greater small N_c limits large N_c. This provides greater unimodal/bimodal separations than Figures 1c and 1d and bimodal concentrations in ndf order (cyan, blue then black) in Figures 3c and 3d. This is the inverse order of Figures 3a and 3b. Figures 3e and 3f also show greater unimodal/bimodal drizzle concentration separations and bimodal drizzle better ndf differentiated than Figures 1e and 1f. The most bimodal lowest ndf octile (black circles) show by far the least drizzle in Figures 3e and 3f whereas for all flights this was a feature only at some Figure 1e diameters. Furthermore, drizzle in bimodal-CCN-associated *clouds* has smaller maximum dia than in unimodal-CCN-associated *clouds* or Figures 1e and 1f. This is especially so for $L_c > 0.35$ g/m^3 where bimodal drizzle is in ndf order from cyan to blue then black at all dia in Figure 3f. Maximum bimodal diameters are also in this same ndf order in Figure 3f.

Table 5 summarizes Figure 3 just as Table 2 summarized Figure 1. Consistent with Table 2, Table 5 shows all 6 low ndf (bimodal) with more mean N_c and complementarily all 6 high ndf (unimodal) with larger mean MD and mean σ and greater mean L_c, N_d and L_d. These trends also follow in height-bias-corrected Table 7 for POST night flights where all 6 N_c ratios are <1 (bimodal bias) and all 6 MD, σ, L_c, N_d and L_d ratios are >1 (unimodal bias). Table 5 shows all mean N_c greater than corresponding Table 2 mean N_c (average 11%) because Figure 2 shows all mean N_{CCN} greater in night flights. Nine of 12 mean MD in Table 5 are smaller than corresponding Table 2 mean MD and all 12 mean σ are smaller than corresponding Table 2 mean σ. Twenty of 24 mean drizzle in Table 5 are less than corresponding Table 2 mean drizzle. This is consistent with smaller MD and especially smaller σ substantially inhibiting collision-coalescence during night flights.

In keeping with lower day N_{CCN} (Figure 2) all Figures 4a and 4b peaks for the 6-day flights are at lower concentrations than Figures 1a, 1b and 3a, 3b. Most importantly Figures 4a and 4b exhibit reverses of Figures 1a and 1b and 3a and 3b because *clouds* associated with unimodal CCN (light colors) display higher peak concentrations

Table 4
Mean Microphysics for the Flight Groups for $L_c > 0.10$ g/m^3

Flights	N	N_c (cm^{-3})	MD (μm)	σ (μm)	L_c (g/m^3)	N_d (L^{-1})	L_d (mg/m^3)	W (m/s)	σ_w (m/s)	hgt(m)	ndf
all 14	141	191	13.75	4.51	0.303	143	19	−0.020	0.488	185	0.293
8 night	**78**	**225**	13.18	3.98	**0.312**	97	14	−0.017	**0.509**	177	0.272
6-day	63	150	**14.45**	**5.14**	0.292	**199**	**24**	**−0.024**	0.463	**195**	**0.319**

Note. N is number of horizontal *cloud* penetrations.

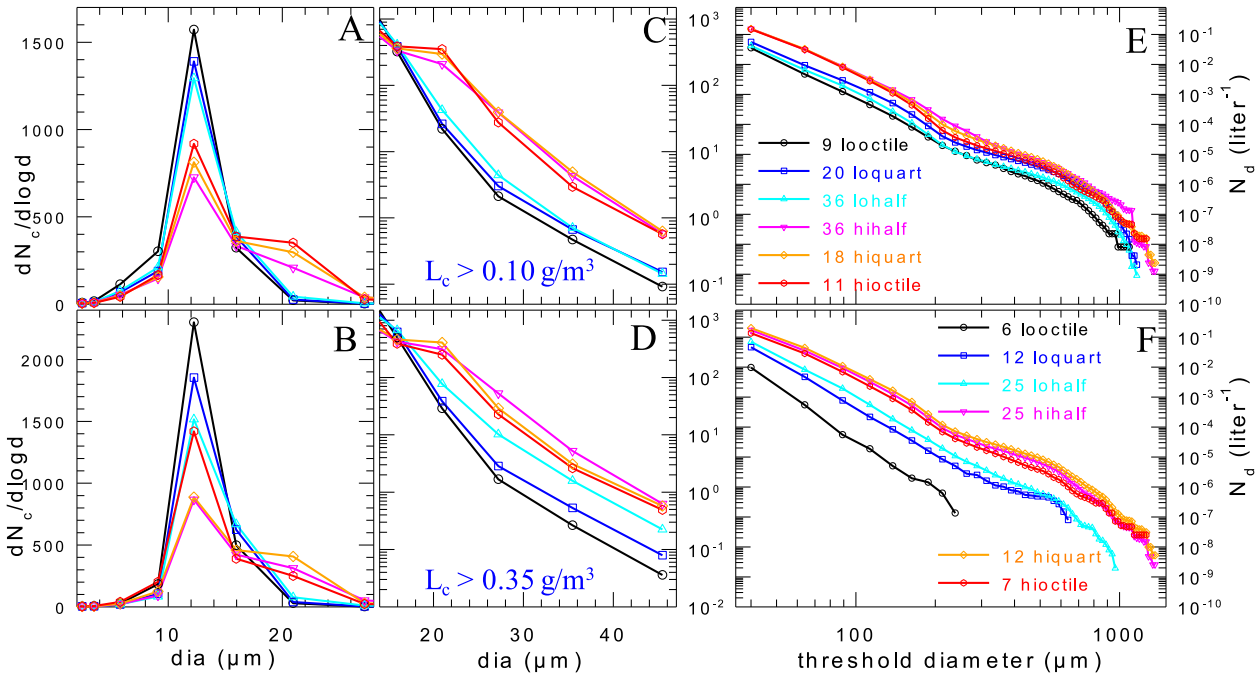

Figure 3. As Figure 1 but for the 78 *clouds* of the 8 night flights. (a, c, e) for 0.1 g/m^3 L_c threshold consider 73 *clouds* and 27 cloud condensation nuclei (CCN) spectra. Only 72 clouds in E legend because median cannot be included in either half division. (b, d, f) for 0.35 g/m^3 L_c threshold consider 50 *clouds* and 23 CCN spectra. Height bias corrected.

Table 5
As Table 2 but for 8 Night Flights

		Low half		High half		Low quartile		High quartile		Low octile		High octile	
$L_c > 0.10$	ndf	−0.049	±0.177	**0.594**	**±0.210**	−0.173	**±0.132**	**0.754**	±0.089	−0.268	**±0.150**	**0.815**	±0.035
	N_c	**259**	±76	191	**±90**	**266**	±71	205	**±98**	**310**	±68	225	**±101**
	MD	12.01	±1.99	**14.42**	**±3.95**	11.78	±1.56	**15.13**	**±4.07**	11.08	±1.83	**15.15**	**±3.88**
	σ	3.43	±0.82	**4.56**	**±1.35**	3.41	±0.66	**4.32**	**±1.41**	3.32	±0.40	**3.86**	**±0.42**
	L_c	0.280	±0.099	**0.328**	**±0.120**	0.277	±0.087	**0.381**	**±0.115**	0.281	±0.101	**0.409**	**±0.109**
	N_d	34	±43	**163**	**±123**	35	±43	**173**	**±119**	15	±15	**169**	**±88**
	L_d	4.4	±7.4	**24**	**±21**	4.9	±8.3	**26**	**±19**	1.8	±2.3	**24**	**±15**
	σ_w	0.509	**±0.146**	**0.525**	±0.098	0.507	**±0.117**	**0.526**	±0.080	0.519	**±0.096**	**0.533**	±0.086
	hgt	158	±93	**199**	**±102**	140	**±101**	**246**	±85	128	**±127**	**234**	±83
$L_c > 0.35$	ndf	−0.038	**±0.212**	**0.670**	±0.149	−0.214	**±0.155**	**0.778**	±0.065	−0.318	**±0.164**	**0.828**	±0.031
	N_c	**283**	±83	204	**±114**	**312**	±76	235	**±117**	**350**	±80	275	**±134**
	MD	13.52	±1.54	**16.30**	**±3.69**	13.08	±0.99	**15.51**	**±3.39**	12.55	±0.90	**14.51**	**±3.67**
	σ	3.20	±1.10	**4.14**	**±1.22**	2.72	±0.47	**3.69**	**±0.49**	2.63	±0.38	**3.56**	**±0.56**
	L_c	0.402	±0.028	**0.441**	**±0.066**	0.396	±0.016	**0.454**	**±0.075**	0.394	±0.011	**0.427**	**±0.053**
	N_d	55	±75	**179**	**±132**	26	±28	**200**	**±114**	6.3	±4.3	**139**	**±63**
	L_d	6.0	±9.0	**26**	**±22**	2.6	±2.9	**29**	**±18**	0.55	±0.38	**19**	**±10**
	σ_w	0.453	**±0.234**	**0.535**	±0.111	0.466	**±0.170**	**0.550**	±0.086	0.540	±0.050	**0.568**	**±0.108**
	hgt	208	±54	**234**	**±89**	200	±61	**240**	**±77**	200	**±84**	**211**	±58

Note. Not height-bias corrected.

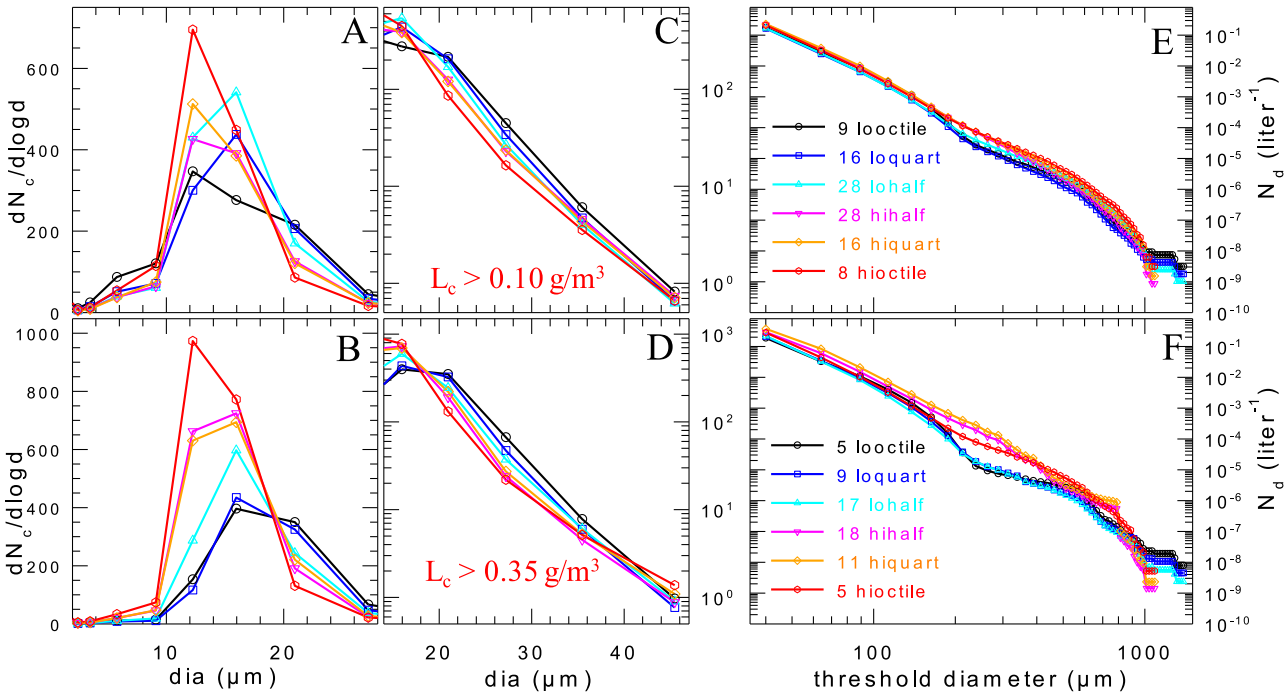

Figure 4. As Figures 1 and 3 but for the 63 *clouds* and 27 cloud condensation nuclei (CCN) spectra of the 6-day flights. (a, c, e) for 0.1 g/m^3 L_c threshold consider 60 *clouds* and 27 CCN spectra. Only 56 clouds displayed in panel (e) legend because 4 clouds at the median cannot be included in either half. (b, d, f) for 0.35 g/m^3 L_c threshold consider 35 *clouds* and 21 CCN spectra. Height bias corrected.

than *clouds* associated with bimodal CCN (dark colors). This result is not predicted from N_{CCN} because bimodal spectra always have higher N_{CCN} than unimodal spectra at low S typical of stratus. In clouds associated with unimodal CCN cloud S goes up to 0.6% in the cleaner day clouds whereas in the higher concentration POST night clouds S in unimodal-associated *clouds* was limited to ∼0.3%. Cloud S associated with day bimodal CCN is limited mostly to the accumulation mode and thus no higher than ∼0.3 to 0.4% depending on which groups of clouds are considered. Thus, Figures 4a and 4b does not resemble H18 Figure 4a for MASE polluted stratus but instead resembles Figure 11 of HN22 for ICE-T clean maritime cumuli. Although the 3 unimodal peaks are at the same 12 μm dia as all six peaks of Figures 1a and 1b and 3a and 3b, unlike those figures the 3 lower concentration bimodal peaks are at larger dia in Figures 4a and 4b. These peak dia differences of the two *cloud* sets make Figures 4a and 4b (especially B) better matches to HN20 Figure 11 for ICE-T than Figures 1a and 1b or Figures 3a and 3b match H18 Figure 4a for MASE. This is because H18 Figure 4a for MASE and HN20 Figure 11 for ICE-T have different dia peaks for the 3 unimodal-CCN and the 3 bimodal-CCN *cloud* sets.

Then at dia larger than the line crossings, *clouds* associated with bimodal CCN exhibit greater concentrations than *clouds* associated with unimodal CCN in Figures 4c and 4d, but these opposite bimodal/unimodal differences are smaller than Figures 1c and 1d or Figures 3c and 3d unimodal/bimodal differences. And unlike Figures 1c and 1d and 3c and 3d the unimodal/bimodal separations diminish or even reverse at largest droplet dia in Figures 4c and 4d. Then Figures 4e and 4f indicates a second unimodal/bimodal set of line crossings because Figures 4e and 4f exhibit more drizzle in *clouds* associated with unimodal CCN than *clouds* associated with bimodal CCN (light colors above dark colors). These day flight drizzle panels are then in the same sense as the drizzle panels of Figures 1 and 3 but with smaller unimodal/bimodal separations.

The day flight summary in Table 6 shows corresponding lower mean N_c than Tables 2 and 5 that average 66% of Table 5 mean N_c and are mostly in the opposite sense with respect to ndf. That is greater mean N_c in unimodal-CCN-associated *clouds* (higher ndf) for 5 of the 6 Table 6 mean N_c comparisons. This is also the case for height-bias-corrected N_c ratios in Table 7 POST day where 5 of 6 mean N_c ratios are greater than 1. Complementary to N_c and in complete opposition to Tables 2 and 5 mean MD in Table 6 is larger in *clouds* associated with bimodal CCN (6 of 6 and also 6 of 6 mean MD ratios are <1 in day Table 7). However, unlike Tables 2 and 5 there are

Table 6
As Tables 2 and 5 but for 6-Day Flights

		Low half		High half		Low quartile		High quartile		Low octile		High octile	
$L_c > 0.10$	ndf	0.195	**±0.134**	**0.443**	±0.107	0.121	**±0.134**	**0.517**	±0.083	0.046	**±0.139**	**0.588**	±0.051
	N_c	**166**	±70	145	**±72**	149	±67	**155**	**±83**	158	±81	**197**	**±83**
	MD	**14.58**	±2.84	13.98	**±3.01**	**14.89**	**±3.17**	13.76	±2.81	**14.14**	**±4.00**	12.26	±1.85
	σ	4.95	**±1.42**	**5.18**	±1.36	5.19	**±1.45**	**5.40**	±1.34	**5.73**	**±1.45**	5.12	±0.93
	L_c	**0.314**	±0.079	0.256	**±0.100**	**0.305**	±0.088	0.260	**±0.099**	**0.291**	±0.114	0.270	**±0.125**
	N_d	172	±133	**222**	**±135**	167	±118	**226**	**±141**	180	±130	**202**	**±137**
	L_d	21	**±19**	**28**	±18	20	±17	**29**	**±19**	24	**±20**	**25**	±16
	σ_w	**0.473**	±0.118	0.468	**±0.168**	**0.462**	**±0.139**	0.436	±0.130	**0.458**	±0.101	0.447	**±0.126**
	hgt	**204**	±66	191	**±70**	**207**	**±84**	196	±65	**214**	**±113**	192	±91
$L_c > 0.35$	ndf	0.164	**±0.155**	**0.403**	±0.115	0.068	**±0.159**	**0.461**	±0.113	−0.044	**±0.122**	**0.569**	±0.055
	N_c	154	±58	**204**	**±74**	126	±28	**197**	**±83**	128	±32	**253**	**±59**
	MD	**16.27**	±2.00	14.82	**±2.52**	**17.00**	±1.20	15.23	**±2.79**	**16.90**	**±1.41**	13.26	±1.06
	σ	**4.84**	**±1.44**	4.53	±1.02	**5.32**	**±1.24**	4.59	±0.89	**5.91**	**±1.18**	4.94	±0.90
	L_c	**0.400**	**±0.037**	0.400	±0.032	**0.408**	**±0.048**	0.406	±0.040	**0.426**	**±0.061**	0.421	±0.056
	N_d	**203**	**±139**	194	±135	207	±96	**231**	**±153**	211	±82	**258**	**±138**
	L_d	25	±25	**42**	**±68**	26	±17	**57**	**±84**	26	±18	**34**	**±18**
	σ_w	**0.504**	**±0.236**	0.478	±0.179	**0.476**	±0.176	0.450	**±0.213**	**0.485**	**±0.188**	0.466	±0.172
	hgt	**229**	**±53**	207	±52	**249**	±61	209	**±65**	**291**	±49	182	**±88**

Note. Not height-bias corrected.

parametric inconsistencies in Table 6 such as mean N_c higher in unimodal *clouds* except $L_c > 0.10$ g/m^3 half, which shows greater mean N_c and larger mean MD in bimodal-CCN-associated *clouds*. This oddity is also shown in Table 7 where day half 0.10 g/m^3 shows both N_c and MD ratios <1, thus noncomplimentary. Furthermore, for 0.10 g/m^3 halves and quartiles mean σ are larger in unimodal *clouds* but mean MD are larger in bimodal *clouds*. This is the same for POST day flights of Table 7 where the only MD or σ ratios greater than 1 occur for half and quartile σ ratios for 0.1 g/m^3 L_c. Opposite of Tables 2 and 5 all mean L_c are greater in bimodal *clouds* of Table 6 and nearly the same in Table 7 where all L_c ratios are <1 except that halves 0.35 g/m^3 L_c ratio is equal to 1. Contrary to Tables 2 and 5 all 6 mean MD (the same in Table 7, all 6-day mean MD ratios <1) and 4 of 6 mean σ (also 4 of 6 mean σ ratios <1 in day Table 7) are larger in bimodal *clouds*. Many Table 6 differences from Tables 2 and 5 reflect the smaller bimodal/unimodal ndf differences for day than for night or all flights in the first rows of these tables.

On the other hand, mostly similar to Tables 2 and 5 there is more drizzle in unimodal-associated *clouds* (higher ndf) in 11 of the 12 Table 6 drizzle comparisons (the same in height-bias-corrected Table 7 for day). However, the day drizzle unimodal/bimodal differences are much less than for all flights of Table 2, or especially for night flights of Table 5. This is the same in Table 7 where 11 of 12-day drizzle ratios are >1, but these ratios are notably smaller than corresponding drizzle ratios in Table 3 for all flights and Table 7 POST night flights.

Table 7 height-bias-corrected night flight unimodal/bimodal ratios compare more favorably to MASE than does Table 3 for all flights because of the similar drizzle ratios for $L_c > 0.1$ g/m^3, especially for octile. However, there are even higher drizzle ratios for night 0.35 g/m^3 for quartiles and especially octiles. POST day *clouds*, however, compare more favorably with ICE-T (HN20) because of the mostly greater unimodal mean N_c (5 of 6 ratios >1) and complementarily larger mean MD (6 of 6) and larger mean σ (4 of 6) in bimodal *clouds* (ratio <1). The 11 of 12-day drizzle ratios that are greater than 1 are, however, less than the drizzle ratios for all POST flights and especially POST night flights and MASE. The POST day flight drizzle ratios >1 are much greater than the opposite ICE-T drizzle ratios <1 that denote more drizzle in bimodal-CCN-associated *clouds*.

Table 7

As Table 3 but for 8 Night Flights and 6-Day Flights of Physics of Stratocumulus Tops and Marine Stratus/Stratocumulus Experiment $L_c > 0.10$ g/m^3 (From Table 1 of H18) and ICE-T $L_c > 0.10$ g/m^3 (From Table 2 of HN20)

	POST night					
	$L_c > 0.10$ g/m^3			$L_c > 0.35$ g/m^3		
	hi/lo half	hi/lo quart	hi/lo octile	hi/lo half	hi/lo quart	hi/lo octile
ndf	0.643	0.913	1.083	0.708	0.992	1.146
N_c	0.765	0.842	0.786	0.765	0.817	0.801
MD	1.106	1.043	1.103	1.152	1.103	1.132
σ	1.291	1.173	1.071	1.246	1.269	1.328
L_c	1.033	1.017	1.089	1.052	1.076	1.064
N_d	3.695	2.743	4.172	2.784	5.186	14.800
L_d	4.441	3.402	5.582	3.485	6.272	17.980
σ_w	1.008	0.977	0.968	1.181	1.180	1.052
hgt	1.257	1.752	1.825	1.125	1.199	1.054
POST Day						
ndf	0.248	0.396	0.542	0.239	0.393	0.613
N_c	0.850	1.016	1.197	1.406	1.739	2.029
MD	0.988	0.947	0.915	0.881	0.853	0.773
σ	1.059	1.051	0.911	0.922	0.844	0.831
L_c	0.849	0.882	0.994	1.000	0.967	0.981
N_d	1.341	1.398	1.199	0.913	1.047	1.203
L_d	1.386	1.499	1.111	1.604	2.061	1.281
σ_w	0.998	0.951	0.992	0.939	0.930	0.957
hgt	0.935	0.946	0.893	0.901	0.840	0.626
	MASE			ICE-T		
ndf	0.550	0.850	1.060	0.680	0.890	1.150
N_c	0.863	0.799	0.761	1.404	1.521	1.879
MD	1.085	1.112	1.144	0.843	0.852	0.862
σ	1.125	1.214	1.286	0.764	0.773	0.856
L_c	1.111	1.225	1.241	0.706	0.750	1.000
N_d	2.004	3.040	4.116	0.374	0.329	0.502
L_d	2.187	3.380	5.065	0.043	0.040	0.958
σ_w/W	0.933	0.867	0.813	0.849	1.062	1.500
hgt	0.797	0.831	1.000	0.796	0.752	0.904
N_d				0.025	0.036	0.015
L_d				0.012	0.013	0.009

Note. ICE-T displays vertical wind, W, rather than standard deviation of W, σ_w, for POST and MASE. ICE-T also includes drizzle measured by a precipitation probe as well as the cloud probe. Ndf shows the difference instead of ratio. POST is height bias corrected.

3.3. Altitude Divisions

Since HN22 found important differences in RICO cumulus cloud measurements among four altitude categories, POST stratus measurements are now divided into two altitude categories. However, to account for typical stratus cloud base altitude variations this division is done according to distance above cloud base of the measurements, height. Figures 5a–5d shows very different small cloud droplet ndf patterns for these two height divisions, which contain equal numbers of *clouds*. Figures 5b and 5d upper heights display larger size distributions as should be

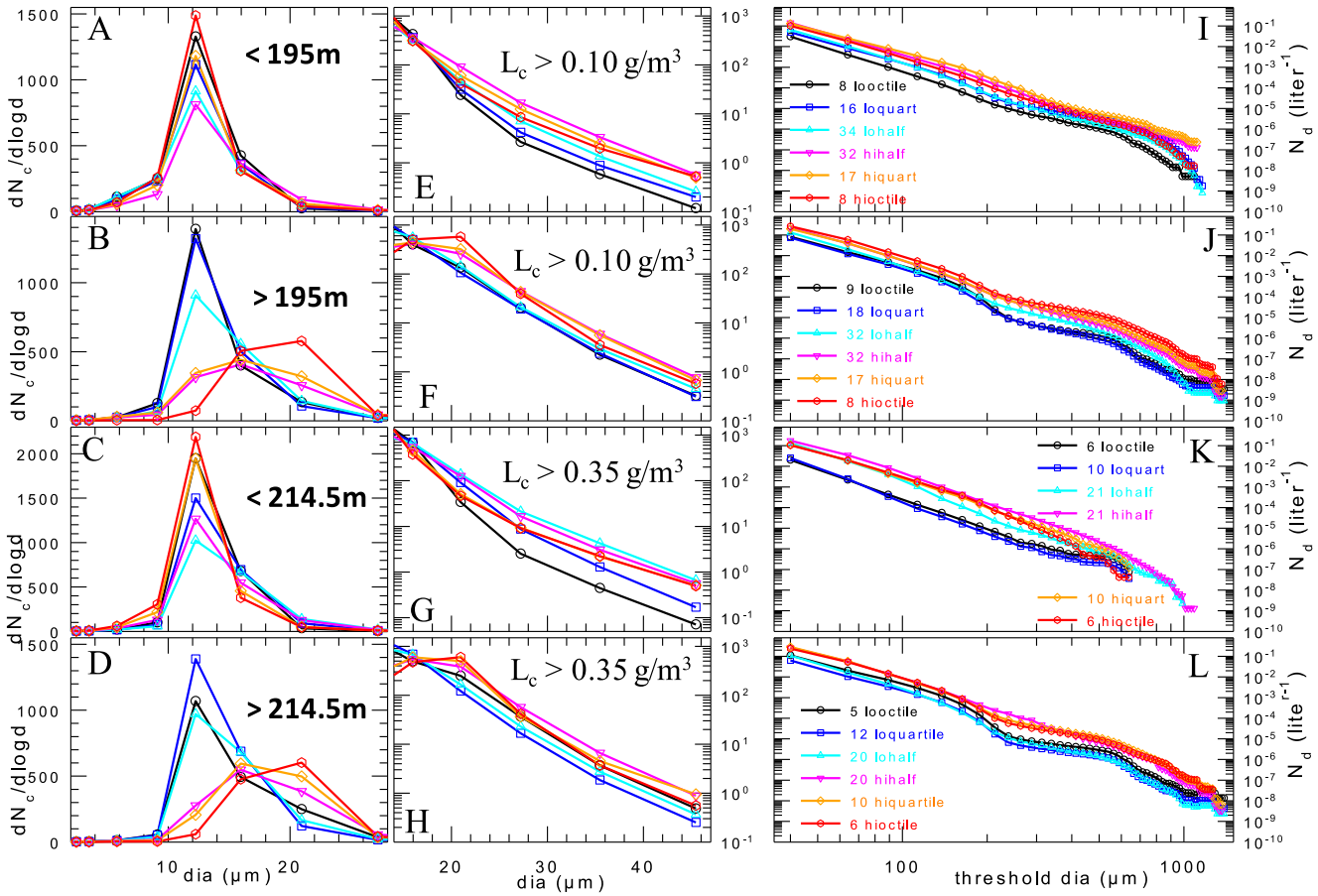

Figure 5. As Figure 1 but cloud measurements are split in half according the within cloud height. Lower (a, e, i, c, g, k) and upper halves (b, f, j, d, h, l) of heights. (a, b, e, f, i, j) use threshold $L_c > 0.10$ g/m^3 with 133 *clouds* and 54 cloud condensation nuclei (CCN) spectra. (a, e, i) Lower half have 35 CCN spectra and 66 *clouds* because median of the 133 *clouds* cannot be included in lower or upper half. (b, f, j) for upper half has 40 CCN and only 64 *clouds* because 2 *clouds* at this ndf median also cannot be included in either ndf half division. (c, g, k, d, h, l) use threshold L_c 0.35 g/m^3 with 85 *clouds* and 44 CCN. (c, g, k) for lower half has 26 CCN but only 42 *clouds* because the median of the 85 *clouds* cannot be included in lower or upper half. (d, h, l) for upper half has 25 CCN and only 40 *clouds* because the one *cloud* at the median of the 85 *clouds* and 2 *clouds* at the ndf median of the 42 upper heights cannot be included in either ndf half. Height bias corrected.

expected due to greater droplet growth at greater heights. Larger sizes are more prominent for unimodal-CCN-associated *clouds* due to lower concentrations but sizes are also shifted for bimodal-CCN-associated *clouds* though not as much shifted due to higher concentrations than in unimodal-CCN-associated clouds. Ndf patterns at upper heights are similar to Figures 1a and 1b with the prominent difference that the lower concentration unimodal light color peaks are at larger dia than lower heights or Figures 1a and 1b. This causes greater bimodal/unimodal size separations at upper heights. This feature provides better matches to MASE H18 Figure 4a. Figures 5a and 5c for lower heights do not exhibit any sort of bimodal/unimodal order except that the most unimodal red octagons display the highest droplet peaks for both L_c thresholds. This is somewhat a reverse of the upper height patterns. However, unlike the upper heights and like Figures 1a and 1b and 3a and 3b all six peaks in Figures 5a and 5c are at the same 12 μm dia. Also, unlike Figures 1a and 1b and 3a and 3b there are no secondary peaks at larger dia in Figures 5a and 5c.

Complementary to Figures 5a–5d three of the four large droplet spectra of Figures 5e–5h show consistently higher concentrations in unimodal-CCN-associated *clouds* at all dia larger than 18 μm. Then all four Figures 5i–5l display more drizzle in unimodal-CCN-associated *clouds*, especially upper heights of Figures 5j and 5l, which unlike Figures 5i and 5k also extend to the largest measured dia. The only slight exception to more unimodal-CCN-associated drizzle is at some dia in Figure 5k. This exception corresponds to the large droplet exception of Figure 5g, which did not display the distinct unimodal/bimodal separations of Figures 5e and 5f or 5h. Another relevant exception for this height and L_c is that the lower left quadrant of Table 8, which summarizes Figures 5c–

Table 8

As Table 3 for All 14 Physics of Stratocumulus Tops Flights but the Measurements Are Divided According to Heights Within the Clouds Where They Were Made Into the Lower Half and Upper Half of Heights

	$L_c > 0.10$ g/m^3					
	Lower heights			Upper heights		
	hi/lo half	hi/lo quart	hi/lo octile	hi/lo half	hi/lo quart	hi/lo octile
ndf	0.415	0.712	0.893	0.514	0.787	1.009
N_c	0.845	0.972	0.992	0.675	0.650	0.595
MD	1.104	1.017	0.932	1.056	1.101	1.227
σ	1.144	1.118	1.105	1.229	1.222	1.081
L_c	1.057	0.992	0.874	0.907	0.984	1.222
N_d	2.165	2.643	3.321	1.666	2.723	3.183
L_d	2.500	3.414	5.595	1.701	2.571	2.967
σ_w	0.991	1.069	1.079	0.963	0.869	0.997
hgt	1.193	1.264	1.468	1.080	1.109	1.154
$L_c > 0.35$ g/m^3						
ndf	0.429	0.766	0.932	0.597	0.850	1.053
N_c	1.130	1.177	1.128	0.712	0.631	0.638
MD	0.944	0.912	0.919	1.140	1.189	1.201
σ	1.067	1.090	1.254	1.158	1.202	0.914
L_c	0.995	0.975	0.961	1.077	1.143	1.183
N_d	1.312	4.436	5.176	2.470	4.443	2.154
L_d	1.623	6.851	6.975	2.746	4.181	2.130
σ_w	1.067	1.114	1.161	1.061	0.988	0.965
hgt	0.885	0.862	0.968	1.071	1.070	1.021

Note. Height-bias corrected.

5g and 5k, has the only Table 8 N_c ratios >1 (unimodal dominance). Of further Figure 5 mention, Figure 5j at dia 300–900 μm displays nearly complete ndf order: from red, to orange, pink, cyan and then similar blue and black (most bimodal) drizzle. Then, corresponding Figure 5b exhibits the only small droplet spectrum with bimodal peaks in ndf order (black, blue then cyan) as well as unimodal peaks in exactly reversed ndf order at 21 μm (red, orange then pink). The latter is also displayed at the other high altitude of Figure 5d.

Corresponding Table 8 row 2 enumerates the much lower N_c ratios (bimodal bias) of the upper heights (right side) than the lower heights (left side) that are so prominently displayed by the much higher bimodal darker color peaks than unimodal lighter color peaks in Figures 5b and 5d. Figures 5a and 5c for the lower heights does not display the bimodal/unimodal separations that provide the low N_c ratios of the right side of Table 8 for upper heights that pertain to Figures 5b and 5d. These upper height N_c ratios <1 are abundantly complemented by larger ratios and thus unimodally biased MD and σ ratios >1 in 11 of the 12 cases in rows 3 and 4 of the right side of Table 8. Nevertheless, the exceptional σ ratio <1 of 0.914 for octile (far right) 0.35 g/m^3 L_c (lower right quadrant) is still greater than the corresponding 0.638 N_c ratio for 0.35 g/m^3 L_c upper heights. This exceptional far right column then consistently has the smallest upper height drizzle ratios of 2.154 and 2.130 except for the 1.666 and 1.701 drizzle ratios of 0.10 g/m^3 L_c upper height half. Lower heights (left side) show 5 of 6 N_c/MD complementarity. However, $L_c > 0.35$ g/m^3 lower height displays opposite N_c/MD complementarity because this is the only Table 8 quadrant (lower left) with more unimodal droplets (N_c ratios >1). Nonetheless, 11 of the 12 Table 8 σ ratios are greater than 1 whereas only 8 of 12 MD ratios are greater than 1. Moreover, 10 of 12 σ ratios are greater than corresponding MD ratios. The two cases with σ ratios less than MD ratios are for both octile upper heights (far right columns), which seemingly consequently display the lowest Table 8 octile drizzle ratios of 3.183, 2.967, 2.154 and 2.130. The $L_c > 0.35$ g/m^3 upper height lower right quadrant of Table 8 with the very lowest 0.914 Table 8 σ ratio, which is the only Table 8 σ ratio <1, shows the very lowest Table 8 octile drizzle ratios of 2.154

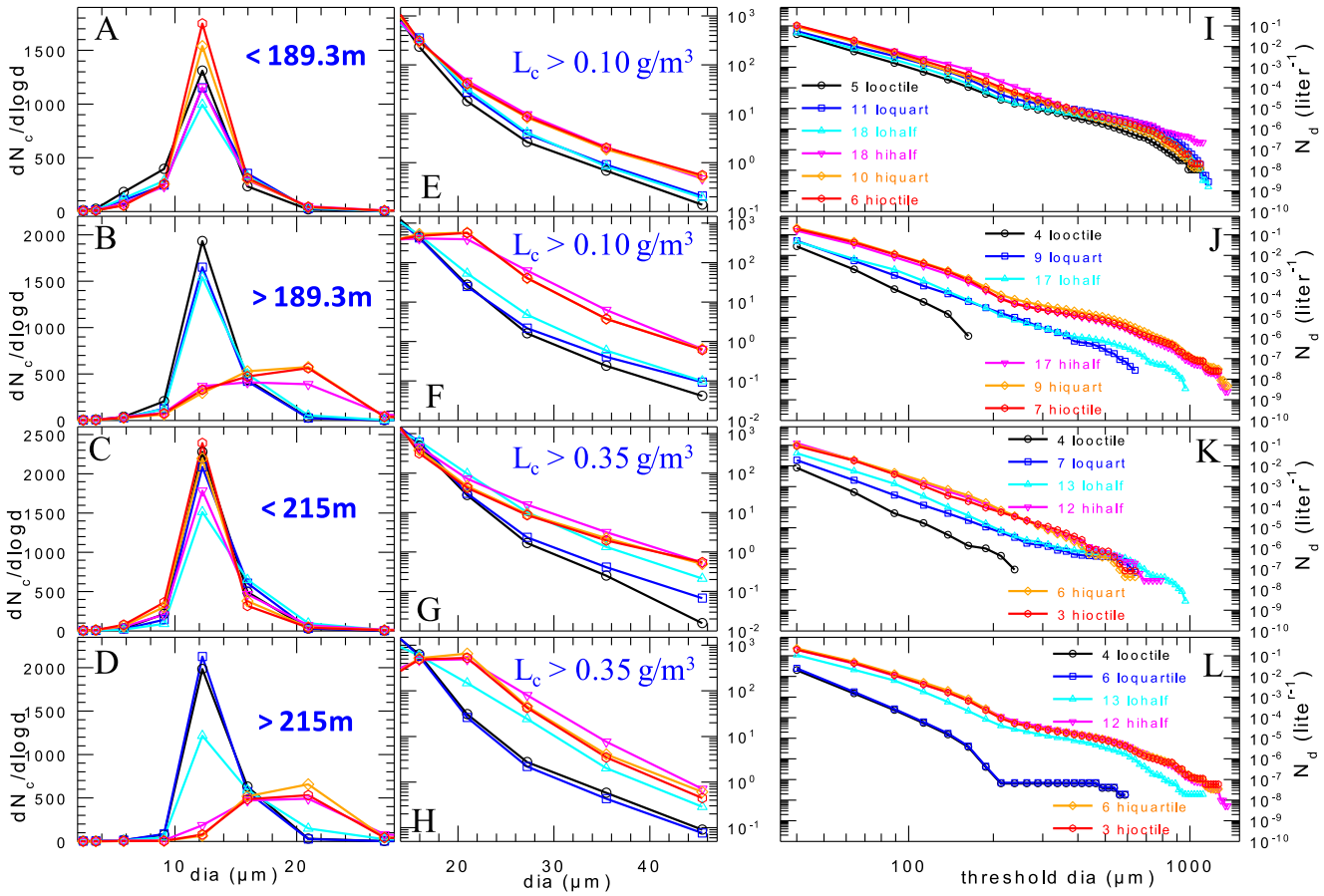

Figure 6. As Figure 3 for the 78 *clouds* of the 8 night flights but like Figure 5 splitting data according to height. (a, b, e, f, i, j) use threshold $L_c > 0.10$ g/m^3 with 73 *clouds* and 27 cloud condensation nuclei (CCN). (a, e, i) lower half has 16 CCN and 36 *clouds* because the median cannot be included in either half height. (b, f, j) for upper half of heights has 19 CCN and 36 *clouds* but only 34 are shown in F legend because 2 *clouds* at this median cannot be counted in either half. (c, g, k, d, h, l) use threshold L_c 0.35 g/m^3 with 50 *clouds* and 23 CCN. (c, g, k) have 14 CCN and 25 *clouds*. (d, h, l) have 11 CCN and 25 *clouds*. Height bias corrected.

and 2.130. These octile drizzle ratios are even lower than all 8 Table 8 quartile drizzle ratios and even lower than the two half drizzle ratios in the upper left quadrant (2.165 and 2.500). Despite all 3 bimodal MD biases (ratio <1) in the lower left quadrant all 6 drizzle ratios are unimodal-biased (ratio >1). This is especially noteworthy for octiles where the 0.919 s lowest Table 8 MD ratio and the very highest 1.254 Table 8 σ ratio lead to the very highest Table 8 N_d and L_d ratios of 5.176 and 6.975, respectively. Thus, broader unimodal-CCN droplet spectra (σ ratio >1) are commensurate with drizzle showing the highest ratios in all 12 columns of Table 8. In the lower right quadrant of Table 8 the highest σ ratio of 1.202 for quartiles fosters the highest drizzle ratios of 4.443 and 4.181 for quartiles while the lowest 0.914 σ ratio for octiles fosters the lowest drizzle ratios of the lower right quadrant for octiles. The preceding nine sentences indicate greater relevance of σ than MD to drizzle production in POST.

Figure 6 for height divisions of the 8 night flights is similar to Figure 5 for height divisions of all 14 flights. For upper height Figures 6b and 6d the larger dia lower concentration unimodal peaks (light colors) are relatively lower than the smaller dia higher concentration bimodal peaks (dark colors) when compared to this difference in Figures 5b and 5d. This is due to the greater low/high ndf differences in the first row of Table 5 than the first row of Table 2. Correspondingly, similar to Figures 5b and 5d the larger dia unimodal distributions provide better overall matches to MASE (H18 Figure 4a) than Figures 3a and 3b for all heights at night. This is because as in Figures 1a and 1b all 6 Figures 3a and 3b peaks are at the same 12 μm dia. Figures 6e–6h and 6j–6l show greater unimodal/bimodal separations than corresponding Figures 5e–5h and 5j–5l, respectively. Unlike Figures 5j–5l, Figures 6j–6l even show bimodals in ndf order at all or most diameters, respectively (cyan, then blue, and then black).

Table 9
As Table 8 but for the 8 Night Flights

	$L_c > 0.10$ g/m^3					
	Lower heights			Upper heights		
	hi/lo half	hi/lo quart	hi/lo octile	hi/lo half	hi/lo quart	hi/lo octile
ndf	0.532	0.829	0.954	0.779	1.015	1.188
N_c	0.980	1.087	0.986	0.663	0.731	0.610
MD	1.016	0.999	1.050	1.147	1.189	1.260
σ	1.048	0.949	0.890	1.407	1.111	1.175
L_c	1.022	1.022	1.019	1.022	1.207	1.192
N_d	2.264	1.674	2.723	3.329	4.255	6.988
L_d	3.015	2.047	8.687	3.367	4.489	7.034
σ_w	1.071	1.124	1.030	0.908	0.933	0.863
hgt	1.277	1.715	3.779	1.191	1.275	1.183
$L_c > 0.35$ g/m^3						
ndf	0.647	0.978	1.099	0.643	0.975	1.088
N_c	1.142	1.090	1.106	0.649	0.492	0.449
MD	0.899	0.929	0.922	1.163	1.353	1.384
σ	1.197	1.284	1.249	1.320	1.346	1.480
L_c	0.972	0.970	0.994	1.120	1.239	1.209
N_d	3.129	5.579	11.272	1.766	9.298	9.881
L_d	3.414	7.571	14.033	1.852	11.059	14.618
σ_w	1.120	1.126	1.113	0.996	1.046	1.360
hgt	0.860	0.932	1.139	1.135	1.149	1.034

Note. Height-bias corrected.

In corresponding Table 9 for night flights the lower right quadrant is somewhat similar to the lower right quadrant of Table 8 in that the highest σ ratio of 1.480 as well as the highest MD ratio of 1.384 for octiles (both are the highest Table 9 MD and σ ratios) lead to the highest lower right quadrant drizzle ratios for octiles. Moreover, this L_d ratio is the highest Table 9 L_d ratio. Meanwhile the lowest σ ratio of 1.32 and the lowest MD ratio of 1.163 for halves foster the lowest drizzle ratios in this lower right quadrant for halves. Moreover, this L_d ratio is the lowest L_d ratio of Table 9. For the lower left quadrant of Table 9 the lowest σ ratio of 1.197 and the lowest MD ratio of 0.899 for halves lead to the lowest drizzle ratios of the lower left quadrant for halves.

All six upper height (right side) corresponding MD ratios and 5 of 6 upper height corresponding σ ratios are greater in Table 9 for night flights than Table 8 for all flights. This probably leads to the Table 9 greater upper height drizzle ratios than corresponding Table 8 upper height drizzle ratios for 10 of the 12 cases. The two exceptions for upper height 0.35 g/m^3 L_c halves in the lower right quadrant are probably due to the smallest upper height MD ratio excess of Table 9 than corresponding Table 8 MD ratio (1.163–1.140 = 0.023). The other five Table 9 over Table 8 upper height MD ratios are greater than 0.088.

At lower heights for 0.10 g/m^3 L_c (upper left quadrant) the only corresponding MD or σ ratio excess of Table 9 over Table 8 is MD octiles (1.050–0.932 = 0.118). This is a reason that this upper left quadrant exhibits the most similar drizzle ratios between Tables 8 and 9 where 3 of the 6 comparisons show higher Table 8 drizzle ratios (both quartiles and N_d octile). This is commensurate with the most similar Tables 8 and 9 corresponding drizzle panels of Figures 5i and 6i, which both exhibit the smallest unimodal/bimodal drizzle differences of Figures 5 and 6, especially Figure 6i for night flights. The other three table quadrants show higher corresponding drizzle ratios in Table 9 than Table 8 except as already noted upper height 0.35 g/m^3 L_c half of the lower right quadrant. This is visualized by the smaller cyan/unimodal (light colors) separation in corresponding Figure 6l compared to Figure 5l. Nevertheless, greater Table 9 than Table 8 drizzle ratios in the other 4 of 6 cases in this lower right

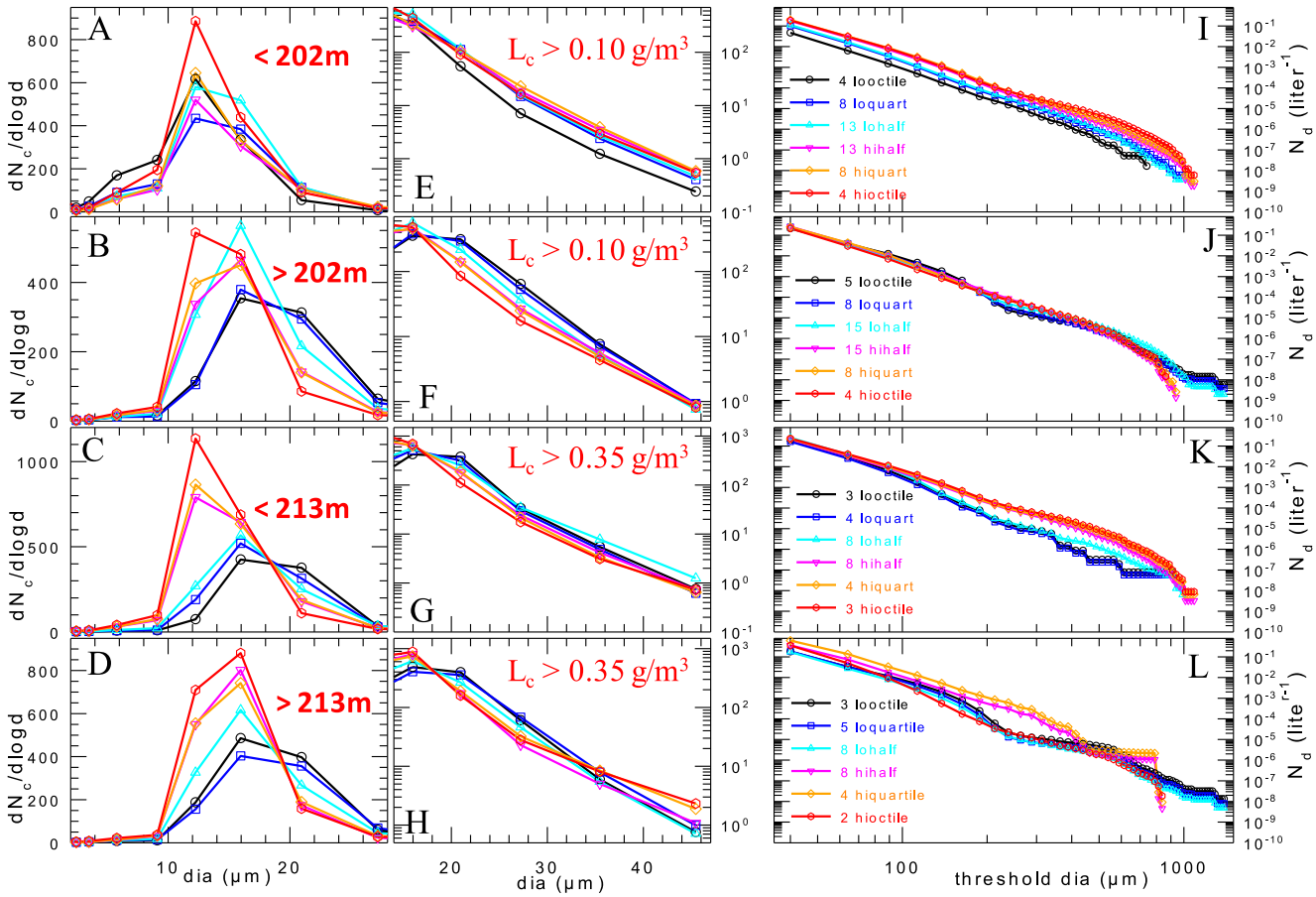

Figure 7. As Figure 4 for the 63 *clouds* and 27 cloud condensation nuclei (CCN) spectra of the 6-day flights but like Figures 5 and 6 splitting data according to height. (a, b, e, f, i, j) use threshold $L_c > 0.10$ g/m^3 with 60 *clouds* and 27 CCN. (a, e, i) lower half of heights has 19 CCN and 30 *clouds* but only 26 show in panel (i) legend because 4 *clouds* at the median cannot be included in either half. (b, f, j) for upper half of heights has 22 CCN and 30 *clouds*. (c, g, k, d, h, l) use threshold L_c 0.35 g/m^3 with 35 *clouds* and 21 CCN. (c, g, k) lower half has 13 CCN and 17 *clouds*. (d, h, l) for upper half has 13 CCN and 17 *clouds*. (k, l) legend show only 16 *clouds* because the median cannot be included in either height half. Height bias corrected.

quadrant are visualized by the greater unimodal/bimodal separation in Figure 6l than Figure 5l. All 12 corresponding drizzle ratios of the other two quadrants (upper height 0.10 g/m^3 L_c upper right quadrant and lower height 0.35 g/m^3 L_c lower left quadrant) are greater in Table 9 than Table 8. This is visualized by the greater unimodal/bimodal separations in Figures 6j and 6k than Figures 5j and 5k, respectively, which correspond to these two table quadrants, respectively. Therefore, upper height night shows greater unimodal/bimodal drizzle excess than upper heights for all flights. For lower heights this is so only for 0.35 g/m^3 L_c where Figure 6k shows greater unimodal/bimodal separation than Figure 5k.

For height-divided day flights Figures 7a–7d small droplets all show ndf patterns fundamentally similar to Figures 4a and 4b for all heights of day flights. For $L_c > 0.10$ g/m^3 the upper heights of Figure 7b show more distinct unimodal/bimodal peak dia differences than lower height Figure 7a. Moreover, Figure 7b shows all spectra at larger dia than lower heights of Figure 7a, which should be expected for greater droplet growth at greater heights. For $L_c > 0.35$ g/m^3 Figures 7c and 7d spectra are similar except for the unimodal (light colors) shift to larger dia at greater height in Figure 7d.

Figures 7f–7h large droplets show bimodal above unimodal up to at least 34 μm whereas Figure 7e shows all unimodal above all bimodal for dia >27 μm. Yet all four Figures 7i–7l drizzle patterns show more unimodal than bimodal drizzle. However, this unimodal/bimodal separation is greater for lower heights of Figures 7i and 7k than Figures 7j and 7l for upper heights. Considering all dia Figure 7i shows the largest unimodal/bimodal separations and almost complete ndf order from red to orange then pink and with black (most bimodal) showing least drizzle

Table 10
As Tables 8 and 9 but for the 6-Day Flights of Physics of Stratocumulus Tops

	$L_c > 0.10$ g/m^3					
	Lower heights			Upper heights		
	hi/lo half	hi/lo quart	hi/lo octile	hi/lo half	hi/lo quart	hi/lo octile
ndf	0.201	0.297	0.375	0.289	0.489	0.667
N_c	0.792	1.053	1.105	0.887	1.207	1.318
MD	1.058	0.965	0.970	0.945	0.892	0.812
σ	1.098	1.157	1.240	1.038	0.910	0.834
L_c	0.923	1.014	1.288	0.802	0.826	0.721
N_d	1.592	1.945	3.977	1.180	1.014	1.003
L_d	1.661	2.162	4.560	1.187	1.061	0.858
σ_w	0.964	0.981	1.108	1.056	0.938	0.823
hgt	0.852	1.047	1.143	0.981	0.922	0.922
$L_c > 0.35$ g/m^3						
ndf	0.148	0.269	0.323	0.357	0.552	0.747
N_c	1.416	1.386	1.698	1.143	1.297	1.387
MD	0.865	0.905	0.816	0.982	0.985	0.901
σ	1.066	1.059	1.044	0.887	0.869	1.081
L_c	1.022	1.037	1.007	1.009	1.057	1.060
N_d	0.862	1.556	1.409	2.400	4.277	2.827
L_d	0.912	1.603	1.429	2.943	5.220	2.459
σ_w	0.831	0.946	0.805	1.169	0.970	1.100
hgt	0.890	0.751	0.666	0.941	0.889	0.873

Note. Height-bias corrected.

at all dia. This ndf order is probably because this L_c and height had the least small droplet ndf organization in Figure 7a and unlike Figures 7f–7h already displayed unimodal above bimodal large droplets in Figure 7e. The other 3-day examples had to undergo two apparent crossovers from more unimodals with smaller dia Figures 7b–7d small cloud droplets to more bimodal Figures 7f–7h large droplets and then more unimodal drizzle in Figures 7j–7l.

Similar to Table 7 for all heights of day flights height-divided day flight Table 10 shows more droplets in unimodal *clouds* (N_c ratios >1) for 10 of the 12 cases. Also, like Table 7 all six corresponding N_c ratios are greater at 0.35 g/m^3 L_c (lower quadrants) than 0.10 g/m^3 L_c (upper quadrants) as is apparent in Figures 7c and 7d than Figures 7a and 7b. The highest N_c ratios for 0.35 g/m^3 L_c lower heights in the lower left quadrant are consistent with the largest small droplet unimodal/bimodal separations of Figure 7c. All six lower height (left side) σ ratios are greater than 1 (unimodal bias) and greater than each of their corresponding MD ratios. Therefore, greater unimodal-biased σ ratios overcome the mostly bimodal-biased MD ratios (5 of 6 ratios <1) to foster greater unimodal drizzle at lower heights (left side 10 of 12 drizzle ratios >1). Specifically, all 3 σ and MD ratios for $L_c > 0.10$ g/m^3 (upper left quadrant) are greater than all 3 σ and MD ratios for $L_c > 0.35$ g/m^3 (lower left quadrant). This seems to lead to all 3 greater N_d and L_d ratios for 0.1 g/m^3 L_c than 0.35 g/m^3 L_c. Additionally, the largest lower height σ excess of 0.10 g/m^3 L_c over 0.35 g/m^3 L_c (1.24–1.044 = 0.196) and the largest MD plus σ excess of 0.10 g/m^3 L_c over 0.35 g/m^3 L_c (2.21–1.86 = 0.35) for octiles apparently caused the largest 0.10 g/m^3 L_c than 0.35 g/m^3 L_c lower height combined drizzle excess of a factor of 3.01. Conversely, the smallest MD plus σ excess of 0.10 g/m^3 L_c over 0.35 g/m^3 L_c (2.122–1.964 = 0.158) for quartiles seems to result in the smallest 0.10 g/m^3 L_c than 0.35 g/m^3 L_c lower height drizzle excess of a factor of 1.300.

For Table 10 upper quadrants ($L_c > 0.1$ g/m^3) all 3 corresponding MD and σ ratios are greater for lower heights (left) than upper heights (right). This seems to cause all 3 N_d and L_d ratios to be greater at lower than upper

heights. Moreover, the largest $L_c > 0.1$ g/m^3 σ ratio of 1.24 and the largest MD plus σ ratios of 2.21 for lower height octiles coupled with the smallest σ ratio of 0.834 and the smallest MD plus σ ratio of 1.646 for $L_c > 0.1$ g/m^3 upper height octile seems to result in the largest $L_c > 0.1$ g/m^3 lower height over upper height combined drizzle ratios of a factor of 4.59. Meanwhile the smallest lower height to upper height σ ratio excess of 0.06 (1.098–1.038) and the smallest MD plus σ ratio excess of 0.173 (2.156–1.983) for halves foster the smallest upper height to lower height drizzle ratio excess of a factor of 1.37 for $L_c > 0.1$ g/m^3.

On the other hand, at upper heights of Table 10 (right side) it is impossible to explain how all six bimodal-biased MD and 4 of 6 bimodal-biased σ ratios can lead to 11 of 12 unimodal-biased drizzle ratios (>1). At least for $L_c > 0.1$ g/m^3 of the Table 10 upper right quadrant the largest MD (0.945) and σ (1.038) ratios for halves are associated with the largest drizzle ratios for halves while the smallest MD (0.812) and σ (0.834) ratios for octiles are associated with the smallest upper right quadrant drizzle ratios. The Table 10 lowest average drizzle ratios of the upper right quadrant (1.05) are envisaged by the smallest unimodal over bimodal drizzle separations in Figure 7j than Figures 7i, 7k, or 7l.

4. Discussion

Figure 1 and Tables 2 and 3 indicate that relationships of CCN modality with droplet and drizzle spectra in POST stratus are similar to those in MASE stratus (H18). These results indicate that cloud processing, which produces accumulation mode particles that make aerosol and CCN bimodality (H85–96, C96-13, NH19), could enhance both indirect aerosol effects (IAE). Higher N_c in *clouds* associated with bimodal CCN would enhance cloud brightening (1st IAE) while less drizzle in clouds associated with bimodal CCN would enhance the cloud lifetime effect (2nd IAE). These apparent cloud processed effects on cloud and drizzle microphysics are then opposite of the bimodal CCN associations in cumulus clouds of ICE-T (H20) and RICO (H22) where bimodal CCN were associated with fewer droplets and more drizzle that seemed to reduce both IAE. However, H18 noted that since all MASE clouds formed in polluted air the apparent different stratus and cumulus cloud relationships with CCN bimodality may also be a function of N_{CCN} differences between polluted MASE and clean ICE-T rather than inherent stratus/cumulus dynamics differences. This is relevant to the fact that Figure 3 and Tables 5 and 7 for POST night flights with higher N_{CCN} (Figure 2) and N_c (Table 4) are even more similar to MASE H18 Figures 4 and 5 and Table 3.

On the other hand, the cleaner midday POST flights presented in Figures 4a and 4b and Tables 6 and 7 better resemble small droplet spectra observed in ICE-T cumuli of HN20 Figure 11. Lower N_c and larger MD and σ in bimodal-CCN-associated *clouds* in Table 6 for POST day flights are mostly similar to ICE-T H20 Table 3. The 5 of 6 lower N_c of *clouds* grown on bimodal CCN in Tables 6 and 7 day tend to reduce 1st IAE in the cleaner midday POST stratus. However, these smaller unimodal/bimodal N_c, MD and σ differences for $L_c > 0.1$ g/m^3 than corresponding ICE-T $L_c > 0.1$ g/m^3 differences would reduce 1st IAE less than ICE-T yet certainly do not enhance 1st IAE as is the case for MASE and POST night.

Although HN20 did not include a corresponding figure to Figures 4c and 4d, HN20 Figure 11 does display line crossings that at dia larger than 20 μm exhibit more droplets in *clouds* associated with bimodal CCN as is explicitly displayed in Figures 4c and 4d. However, Figures 4e and 4f exhibit less drizzle in *clouds* associated with bimodal CCN than in *clouds* associated with unimodal CCN (light above dark). Since these drizzle drop plots are opposite of ICE-T cumuli, HN20 Figures 12 and 13, they are then similar to Figures 1e and 1f and 3e and 3f and H18 Figure 5 for MASE. Figures 4e and 4f, however, show smaller unimodal/bimodal separations than those figures. At any rate Figures 4c–4f indicate a second set of line crossings that suggest that higher concentrations of large cloud droplets in *clouds* associated with bimodal CCN inhibit the formation of drizzle drops. This is analogous to observations of lower large cloud droplet concentrations that are due to higher concentrations of small cloud droplets. This fundamental aspect of cloud physics is abundantly exhibited in H18 Figure 4 for MASE, H20 Figure 11 for ICE-T, and Figures 1a–1d, 3a–3d, 4a–4d, 5b and 5d, 6b and 6d and 7b–7d for POST. But the notion that high concentrations of large cloud droplets could inhibit drizzle has not been previously reported.

Tables 6 and 7 for day flights also exhibit higher N_d and L_d in *clouds* associated with unimodal CCN for 11 of 12 comparisons. However, none of the drizzle differences in Table 6 for day flights exceed a factor of 2 whereas none of these drizzle differences in Table 2 for all 14 POST flights are less than a factor of 2 and many drizzle differences in Table 5 for POST night flights are an order of magnitude. Thus, bimodal CCN in these POST stratus

enhance 2nd IAE to a much greater extent in the more polluted night *clouds* than in the clean day *clouds*. Nevertheless, bimodal CCN in POST stratus, even clean POST stratus, never seemed to reduce the cloud lifetime effect as seemed to happen in ICE-T cumuli (HN20) and RICO cumuli (HN22).

Figures 5a–5d and 6a–6d demonstrate that the impact of CCN modality is not fully developed at the smaller droplet sizes of lower heights. CCN modality effects prevail only at the greater heights that are actually more relevant to 1st IAE. The lower unimodal/bimodal ratios for N_c at upper heights than lower heights in Tables 8 and 9 for both L_c thresholds further support greater enhancement of 1st IAE in more polluted clouds, especially at higher L_c where N_c is always greater for all flights and for night flights. However, since the polluted clouds in POST prevailed when there was less sunlight this would seem to preclude 1st IAE. Conversely, since all MASE flights occurred during the middle of daylight hours, polluted stratus are certainly not restricted to hours of limited sunlight. It is not evident that the levels of pollution in POST were related to time of day. For the same reason, Figures 7a–7d show that the possible reduction of 1st IAE by bimodal CCN in cleaner POST stratus also prevails at the more relevant greater cloud heights. Table 10 shows that the predominance of a bimodal CCN effect on IAE depends on the L_c threshold but Table 6 shows that unlike night flights N_c is not always greater at higher L_c.

Figures 5i–5l, 6i–6l and 7i–7l show that drizzle suppression by bimodal CCN prevails at all altitudes. But drizzle suppression is more prevalent at higher altitudes in the more polluted nighttime clouds of Figures 6i–6l whereas the clean daytime clouds of Figures 7i–7l show greater drizzle suppression at lower heights and minimal suppression at greater heights. Tables 8 and 9 do not show much of a drizzle suppression difference with height or L_c but Table 10 for day flights shows greater drizzle suppression at lower heights for $L_c > 0.10$ g/m^3 yet more drizzle suppression at greater heights for $L_c > 0.35$ g/m^3.

High magnitude negative R and low P2 for N_c with ndf and complementary high positive R and low P2 for MD with ndf in Table S2 in Supporting Information S1 for all flights and night flights plentifully support the bimodality enhancement of 1st IAE in POST, especially the greater R and lower P2 for night flights. Table S2 in Supporting Information S1 provides weaker support for bimodality reduction of 1st IAE in day flights. Even greater magnitude R and lower P2 in spite of fewer data in Tables S3 and S4 in Supporting Information S1 for upper heights solidifies the enhancement of 1st IAE for POST, especially the night flights. The much higher R and lower P2 for drizzle-ndf provides strong support for bimodal CCN enhancement of 2nd IAE. Table S3 in Supporting Information S1 provides support for 2nd IAE enhancement in day flights at lower heights that is visible in Figures 7i and 7k.

The fact that all POST flights resemble the MASE results shows the dominance of the POST night flights (Figure 3) over the POST day flights (Figure 4) by the larger number of night flights (8–6) with higher N_c. The fact that day flights show some drizzle suppression rather than lower night drizzle concentrations causes the overall POST drizzle suppression. These POST results indicate that the effects of bimodal CCN (often caused by cloud processing) on IAE depend both on the concentration levels and cloud dynamic differences between stratus and cumulus clouds. The POST bimodal CCN impacts on drizzle indicate a negative relationship between low S CCN and drizzle. Analogously the positive relationships between bimodality and drizzle in ICE-T (HN20) and RICO (HN22) suggest a positive relationship between low S CCN and drizzle.

As in any environment, throughout POST N_{CCN} at all S are positively related to N_c; greater N_{CCN} produce greater N_c. This is not so for ndf where lower values are related to higher N_c for all POST flights (Figure 1) and POST night flights (Figure 3) but for POST day flights (Figure 4) higher ndf is associated with more N_c. Lower ndf mean relatively more low S $N_{CCN.}$ Thus, ndf is more relevant than any N_{CCN} because cloud S is not necessarily known. Lower W of stratus largely confines cloud S to the accumulation mode. The greater accumulation mode concentrations of low ndf bimodal CCN thus produce greater N_c than occur in clouds formed on unimodal CCN. This would enhance 1st IAE while the accompanying smaller MD and σ would inhibit coalescence and thus enhance 2nd IAE. Higher ndf with fewer low S CCN allow higher cloud S but not higher N_c. This will allow larger MD and more diverse S CCN to activate thus producing more diverse droplet sizes and then larger σ. H18 demonstrated this for MASE with an adiabatic computer model. Greater MD and σ in *clouds* associated with unimodal CCN better promote autoconversion to drizzle. Opposite cumulus observations are more difficult to explain. Higher W of cumuli can result in extremely high cloud S, especially for unimodal CCN due to the lack of low S CCN that provide lower S limits, which can restrict N_c of clouds associated with bimodal CCN but not clouds associated with unimodal CCN. Lower N_c in bimodal-associated cumuli can lead to larger droplets more likely to precipitate.

Throughout this analysis relationships have been noted between droplet MD and σ with drizzle. The third paragraph of Section 3.3 details these relationships regarding Table 8 for all POST flights while the 5th, 6th and 7th paragraphs of Section 3.3 do so for POST night flights. In the majority of these examples σ seems to have a greater apparent influence on drizzle than MD. The third from the last paragraph of Section 3.3 demonstrates that unimodal-biased σ ratios overcome bimodal-biased MD ratios to promote unimodal-biased drizzle in Table 10 for cleaner day flights. H18 also noted this σ over MD influence on drizzle in MASE because more diverse droplet spectra should promote autoconversion.

5. Conclusions

High-resolution extended range CCN spectra comparisons with cloud and drizzle microphysics measurements in the POST stratus field investigation are consistent with observations in the MASE stratus cloud field investigation (HN18). These results show that bimodal CCN spectra commonly observed in cloudier air masses (H85-96; C96-13) are associated with higher cloud droplet concentrations, N_c, smaller droplets, MD, narrower droplet spectra, smaller σ, and less drizzle compared to *clouds* associated with unimodal CCN spectra. All of these observations are opposite of analogous observations in two cumulus cloud field investigations, ICE-T (HN20) and RICO (HN22). Results of these four investigations suggest that cloud processing of aerosol that produces the accumulation mode tends to enhance both IAE (cloud brightening and cloud lifetime) in stratus but reduce both IAE in cumuli.

However, late afternoon/evening (night) flights, which occurred with higher N_{CCN} and N_c, more explicitly and intensely exhibited the MASE observations. POST midday flights with lower N_{CCN} and N_c exhibit mostly opposite cloud droplet microphysics that are more similar to the cumulus observations (HN20 and HN22). However, midday drizzle did not exhibit the bimodality enhancement of ICE-T (HN20) and RICO (HN22) but rather bimodal drizzle suppression though not to the extent of the POST night flights or MASE (HN18).

There are notable differences when cloud and drizzle measurements are divided according to distance above cloud base, height. For all flights and night flights measurements at greater heights more intensely exhibit the differences accorded to CCN modality whereas at lower heights these differences, especially for small cloud droplets, are not observed. Larger droplets and drizzle exhibit the same differences according to CCN modality at both altitude divisions but these differences are greater at greater heights.

Midday flights in cleaner air also display more intense differences at greater heights for small droplets, but the differences with height are not as great as for night flights and depend on the L_c threshold of the measurements. However, at large cloud droplet sizes there are only very small concentration differences according to CCN modality. But drizzle is more distinctly suppressed in clouds associated with bimodal CCN at lower heights. Greater heights better exhibit the second crossover between unimodal and bimodal associated droplet and drop concentrations that suggest that greater concentrations of large cloud droplets suppress drizzle.

Data Availability Statement

[Dataset] POST data used in this manuscript are available at the NCAR-RAF websites https://data.eol.ucar.edu/master_lists/generated/post/. ICE-T and RICO data can also be found at this website with the suffix icet and rico substituted for post. MASE data can be found at https://www.arm.gov/under/arm-iop/2005/pye/mase/senum-cip/.

Acknowledgments
NSF ATM-0734441 supported the POST CCN measurements. Herman Gerber organized POST. CIRPAS pilots, ground crew and scientists provided an ideal platform for the superbly executed flights and provided the cloud microphysics data. CCN measurements referenced here were supported by U.S. DOE Grants DE-FB02-05ER63999 and DE-SC0009162. NSF AGS-1940645 supported the POST analysis presented here.

References

Albrecht, B. A. (1989). Aerosols, cloud microphysics and fractional cloudiness. *Science*, *245*(4923), 1227–1230. https://doi.org/10.1126/science.245.4923.1227

Baumgardner, D. (1983). An analysis and comparison of five water droplet measuring instruments. *Journal of Climate and Applied Meteorology*, *22*(5), 891–910. https://doi.org/10.1175/1520-0450(1983)022<0891:aaacof>2.0.co;2

Birmili, W., Wiedensohler, A., Heintzenberg, J., & Lehmann, K. (2001). Atmospheric particle number size distributions in central Europe: Statistical relations to air masses and meteorology. *Journal of Geophysical Research*, *106*(D23), 32005–32018. https://doi.org/10.1029/2000JD000220

Carman, J. K., Rossiter, D. L., Khelif, D., Jonsson, H. H., Faloona, I. C., & Chuang, P. Y. (2012). Observational constraints on entrainment and the entrainment interface layer in stratocumulus. *Atmospheric Chemistry and Physics*, *12*(22), 11135–11152. https://doi.org/10.5194/acp-12-11135-2012

Christensen, M. W., Jones, W. K., & Stier, P. (2020). Aerosols enhance cloud lifetime and brightness along the stratus-to-cumulus transition. *Proceedings of the National Academy of Science, USA*, *117*(30), 17591–17598. https://doi.org/10.1073/pnas.1921231117

Christensen, M. W., Peng, W., Varble, A. C., Xiao, H., & Fast, J. D. (2024). Aerosol-induced closure of marine cloud cells: Enhanced effects in the presence of precipitation. *Atmospheric Chemistry and Physics*, *24*(11), 6455–6476. https://doi.org/10.5194/acp-24-6455-2024

Clarke, A. D., Eisele, F., Kapustin, V. N., Moore, K., Tanner, D., Mauldin, L., et al. (1999). Nucleation in the equatorial free troposphere: Favorable environments during PEM-Tropics. *Journal of Geophysical Research*, *104*(C99), 5735–5744. https://doi.org/10.1029/98JD02303

Clarke, A. D., Freitag, S., Simpson, R., Hudson, J. G., Howell, S., Brekhovskikh, V., et al. (2013). Free troposphere as the dominant source of CCN in the equatorial Pacific boundary layer: Long-range transport and teleconnections. *Atmospheric Chemistry and Physics*, *13*(15), 7511–7529. https://doi.org/10.5194/acp-13-7511-2013

Clarke, A. D., Li, Z., & Litchy, M. (1996). Aerosol dynamics in the equatorial Pacific marine boundary layer: Microphysics, diurnal cycles and entrainment. *Journal of Geophysical Research*, *23*(C96), 733–736. https://doi.org/10.1029/96GL00778

Clarke, A. D., Shinozuka, Y., Kapustin, V. N., Howell, S., Huebert, B., Doherty, S., et al. (2004). Size distributions and mixtures of dust and black carbon aerosol in Asian outflow: Physiochemistry and optical properties. *Journal of Geophysical Research*, *109*(C4), D15S09. https://doi.org/10.1029/2003JD004378

Clarke, A. D., Varner, J. L., Eisele, F., Mauldin, R. L., Tanner, D., & Litchy, M. (1998). Particle production in the remote marine atmosphere: Cloud outflow and subsidence during ACE 1. *Journal of Geophysical Research*, *103*(C98), 16397–16409. https://doi.org/10.1029/97JD02987

Covert, D. S., Kapustin, V. N., Bates, T. S., & Quinn, P. K. (1996). Physical properties of marine boundary layer aerosol particles of the mid-Pacific in relation to sources and meteorological transport. *Journal of Geophysical Research*, *101*(D3), 6919–6930. https://doi.org/10.1029/95JD03068

Douglas, A., & L'Ecuyer, T. (2020). Quantifying cloud adjustments and radiative forcing due to aerosol-cloud interactions in satellite observations of warm marine clouds. *Atmospheric Chemistry and Physics*, *20*(10), 6225–6241. https://doi.org/10.5194/acp-20-6225-2020

Feingold, G., Kreidenweis, S. M., Stevens, B., & Cotton, W. R. (1996). Numerical simulations of stratocumulus processing of cloud condensation nuclei through collision-coalescence. *Journal of Geophysical Research*, *101*(D16), 21391–21402. https://doi.org/10.1029/96JD01552

Garrett, T. J., & Hobbs, P. V. (1995). Long-range transport of continental aerosols over the Atlantic Ocean and their effects on cloud structures. *Journal of Geophysical Research*, *52*(16), 2977–2984. https://doi.org/10.1175/1520-0469(1995)052<2977:lrtoca>2.0.co;2

Gerber, H., Frick, G., Malinowski, S. P., Jonsson, H., Khelif, D., & Krueger, S. K. (2013). Entrainment rates and microphysics in POST stratocumulus. *Journal of Geophysical Research: Atmospheres*, *118*(21), 12094–12109. https://doi.org/10.1002/jgrd.50878

Gryspeerdt, E., Povey, A. C., Grainger, R. G., Hasekamp, O., Hsu, N. C., Mulcahy, J. P., et al. (2023). Uncertainty in aerosol-cloud radiative forcing is driven by clean conditions. *Atmospheric Chemistry and Physics*, *23*(7), 4114–4122. https://doi.org/10.5194/acp-23-4115

Hoffmann, D. J. (1993). Twenty years of balloon-borne tropospheric aerosol measurements at Laramie, Wyoming. *Journal of Geophysical Research*, *98*(D7), 12753–12766. https://doi.org/10.1029/93JD00466

Hoppel, W. A., Fitzgerald, J. W., Frick, G. M., Larson, R. E., & Mack, E. J. (1990). Aerosol size distributions and optical properties found in the marine boundary layer over the Atlantic Ocean. *Journal of Geophysical Research*, *95*(D4), 3659–3686. https://doi.org/10.1029/JD095iD04p03659

Hoppel, W. A., Fitzgerald, J. W., & Larson, R. E. (1985). Aerosol size distributions in air masses advecting off the East Coast of the United States. *Journal of Geophysical Research*, *90*(D1), 2365–2379. https://doi.org/10.1029/JD090iD01p02365

Hoppel, W. A., Frick, G. M., & Fitzgerald, J. W. (1996). Deducing droplet concentration and supersaturation in marine boundary layer clouds from surface aerosol measurements. *Journal of Geophysical Research*, *101*(D21), 26553–26565. https://doi.org/10.1029/96jd02243

Hoppel, W. A., Frick, G. M., Fitzgerald, J. W., & Larson, R. E. (1994). Marine boundary layer measurements of new particle formation and the effects nonprecipitating clouds have on aerosol size distribution. *Journal of Geophysical Research*, *99*(D7), 14443–14459. https://doi.org/10.1029/94JD00797

Hoppel, W. A., Frick, G. M., & Larson, R. E. (1986). Effect of nonprecipitating clouds on the aerosol size distribution in the marine boundary layer. *Geophysical Research Letters*, *13*(2), 125–128. https://doi.org/10.1029/GL013i002p00125

Hudson, J. G. (1989). An instantaneous CCN spectrometer. *Journal of Atmospheric and Oceanic Technology*, *6*(6), 1055–1065. https://doi.org/10.1175/1520-0426(1989)006<1055:AICS>2.0.CO;2

Hudson, J. G., & Noble, S. (2014a). Low altitude summer/winter microphysics, dynamics and CCN spectra of northeastern Caribbean small cumuli; and comparisons with stratus. *Journal of Geophysical Research: Atmospheres*, *119*(9), 5445–5463. https://doi.org/10.1002/2013JD021442

Hudson, J. G., & Noble, S. (2014b). CCN and vertical velocity influences on droplet concentrations and supersaturations in clean and polluted stratus clouds. *Journal of the Atmospheric Sciences*, *71*(1), 312–331. https://doi.org/10.1175/JAS-D-13-086.1

Hudson, J. G., & Noble, S. (2020). CCN spectral shape and cumulus cloud and drizzle microphysics. *Journal of Geophysical Research: Atmospheres*, *125*(1), e2019JD031141. https://doi.org/10.1029/2019JD031141

Hudson, J. G., & Noble, S. (2021). Cumulus cloud and drizzle microphysics relationships with complete CCN spectra. *Journal of Geophysical Research: Atmospheres*, *126*(15), e2021JD034966. https://doi.org/10.1029/2021JD034966

Hudson, J. G., & Noble, S. (2022). CCN spectral modality compared to droplet spectra and drizzle in RICO cumuli. *Journal of Geophysical Research: Atmospheres*, *127*(24), e2022JD037189. https://doi.org/10.1029/2022JD037189

Hudson, J. G., Noble, S., & Jha, V. (2010). Stratus cloud supersaturations. *Geophysical Research Letters*, *37*(21), L21813. https://doi.org/10.1029/2010GL045197

Hudson, J. G., Noble, S., & Tabor, S. (2018). CCN spectral shape and stratus cloud and drizzle microphysics. *Journal of Geophysical Research: Atmospheres*, *123*(17), 9635–9651. https://doi.org/10.1029/2017JD027865

Intergovernmental Panel on Climate Change 2014. (2021). WGI 5th & 6th assessment, final.

Jensen, T. L., Kreidenweis, S. M., Kim, Y., Sievering, H., & Pszenny, A. (1996). Aerosol distributions in the north Atlantic marine boundary layer during Atlantic stratocumulus transition experiment/marine aerosol and gas exchange. *Journal of Geophysical Research*, *101*(D2), 4455–4467. https://doi.org/10.1029/95JD00506

Kleinman, L. I., Daum, P. H., Lee, Y.-N., Lewis, E. R., Sedlacek III, A. J., Senum, G. I., et al. (2012). Aerosol concentration and size distribution measured below, in, and above cloud from the DOE G-1 during VOCALS-Rex. *Atmospheric Chemistry and Physics*, *12*(1), 207–223. https://doi.org/10.5194/acp-12-207-2012

Kogan, Z. N., Kogan, Y. L., & Lilly, D. K. (1996). Evaluation of sulfate aerosols indirect effect in marine stratocumulus clouds using observation-derived cloud climatology. *Geophysical Research Letters*, *23*(15), 1937–1940. https://doi.org/10.1029/96gl01793

Lenschow, D. H., & Spyers-Duran, P. (1989). Measurement techniques: Air motion sensing. *NCAR RAF Bulletin*, *23*, 8151. Retrieved from http://opensky.ucar.edu/islandora/object/archives

Masson-Delmotte, V., Zhai, P., Pirani, A., Connors, S. L., Pean, C., Berger, S., et al. (Eds.). (2021). Climate Change 2021*: The physical science basis, contribution of working group 1 to the sixth assessment report of the intergovernmental panel on climate Change*. Cambridge University Press. https://doi.org/10.1017/9781009157896

Modini, R. L., Frossard, A. A., Ahlm, L., Russell, L. M., Corrigan, C. E., Roberts, G. C., et al. (2015). Primary marine aerosol-cloud interactions off the coast of California. *Journal of Geophysical Research*, *120*(9), 4282–4303. https://doi.org/10.1002/2014JD022963

Mulmenstadt, J., & Feingold, G. (2018). The radiative forcing of aerosol-cloud interactions in liquid clouds: Wrestling and embracing uncertainty. *Current Climate Change Reports*, *4*(1), 23–40. https://doi.org/10.1007/s40641-018-0089-y

NCAR-RAF. (2022). [Dataset]. https://data.eol.ucar.edu/master_lists/generated/post/

Noble, S., & Hudson, J. G. (2019). Effects of continental clouds on surface Aitken and accumulation modes. *Journal of Geophysical Research: Atmospheres*, *124*(10), 5479–5502. https://doi.org/10.1029/2019JD030297

O'Dowd, C. D., Lowe, J. A., & Smith, M. H. (1999). Observations and modeling of aerosol growth in marine stratocumulus—Case study. *Atmospheric Environment*, *33*(18), 3053–3062. https://doi.org/10.1016/S1352-2310(98)00213-1

Platnick, S., & Twomey, S. (1994). Determining the susceptibility of cloud albedo to changes in droplet concentration with the Advanced Very High Resolution Radiometer. *Journal of Applied Meteorology*, *33*(3), 334–347. https://doi.org/10.1175/520-0450(1994)033<0334:DTSOCA>2.0.CO;2

Rosenfeld, D., Zhu, Y., Wang, M., Zeng, Y., Goren, T., & Yu, S. (2019). Aerosol-driven droplet concentrations dominate coverage and water of oceanic low-level clouds. *Science*, *363*(6427), eaav0566. https://doi.org/10.1126/science.aav0566

Shingler, T., Dey, S., Sorooshian, A., Brechtel, F. J., Wang, Z., Metcalf, A., et al. (2012). Characterization and airborne deployment of a new counterflow virtual impactor inlet. *Atmospheric Measurement Technology*, *5*(6), 1259–1269. https://doi.org/10.5194/amt-5-1259-2012

Svenningsson, B., Hansson, H. C., Martinsson, B., Wiedensohler, A., Swietlicki, E., Cederfelt, S. I., et al. (1997). Cloud droplet nucleation scavenging in relation to the size and hygroscopic behaviour of aerosol particles. *Atmospheric Environment*, *31*(16), 2463–2475. https://doi.org/10.1016/S1352-2310(96)00179-3

Tomlinson, J. M., Li, R., & Collins, D. R. (2007). Physical and chemical properties of the aerosol within the southeastern Pacific marine boundary layer. *Journal of Geophysical Research*, *112*(D12), D12211. https://doi.org/10.1029/2006JD007771

Tunved, P., Hansson, H.-C., Kulmala, M., Aalto, P., Viisanen, Y., Karlsson, H., et al. (2003). One year boundary layer aerosol size distribution data from five Nordic background stations. *Atmospheric Chemistry and Physics*, *3*(6), 2183–2205. https://doi.org/10.5194/acp-3-2183-2003

Twomey, S. (1977). The influence of pollution on the shortwave albedo of clouds. *Journal of the Atmospheric Sciences*, *34*(7), 1149–1152. https://doi.org/10.1175/1520-0469(1977)034<1149:tiopot>2.0.co;2

Van Dingenen, R., Raes, F., & Jensen, N. R. (1995). Evidence for anthropogenic impact on number concentration and sulfate content of cloud-processed aerosol particles over the North Atlantic. *Journal of Geophysical Research*, *100*(D10), 21057–21067. https://doi.org/10.1029/95JD02141

Wall, C. J., Storelvmo, T., & Possner, A. (2023). Global observations of aerosol indirect effects from marine liquid clouds. *Atmospheric Chemistry and Physics*, *23*(20), 1312–13141. https://doi.org/10.5194/acp-23-13125-2023

Warren, S. G., Hahn, C. J., London, J., Chervin, R. M., & Jenne, R. L. (1988). *Global distribution of total cloud cover and cloud type amounts over the ocean*. NCAR Technical Note NCAR/TN-317+STR.

Weber, R. J., Marti, J. J., McMurry, P. H., Eisele, F. L., Tanner, D. J., & Jefferson, A. (1997). Measurements of new particle formation and ultrafine particle growth rates at a clean continental site. *Journal of Geophysical Research*, *102*(D4), 4375–4385. https://doi.org/10.1029/96JD03656

Weingartner, E., Nyeki, S., & Baltensperger, U. (1999). Seasonal and diurnal variation of aerosol size distributions ($10 < D < 750$ nm) at a high-alpine site (Jungfraujoch 3580 m asl). *Journal of Geophysical Research*, *104*(D21), 26809–26820. https://doi.org/10.1029/1999JD900170

Yang, M., Huebert, B. J., Blomquist, B. W., Howell, S. G., Shank, L. M., McNaughton, C. S., et al. (2011). Atmospheric sulfur cycling in the southeastern Pacific – Longitudinal distribution, vertical profile, and diel variability observed during VOCALS-Rex. *Atmospheric Chemistry and Physics*, *11*(10), 5079–5097. https://doi.org/10.5194/acp-11-5079-2011

References From the Supporting Information

Leaitch, W. R., Banic, C. M., Isaac, G. A., Couture, M. D., Liu, P. S. K., Gultepe, I., et al. (1996). Physical and chemical observations in marine stratus during the 1993 North Atlantic Regional Experiment: Factors controlling cloud droplet number concentrations. *Journal of Geophysical Research*, *101*(D22), 29123–29135. https://doi.org/10.1029/96jd01228

Morales, R., & Nenes, A. (2010). Characteristic updrafts for computing distribution-averaged cloud droplet number, autoconversion rate and effective radius. *Journal of Geophysical Research*, *115*(D18), D18220. https://doi.org/10.1029/2009JD013233

Peng, Y., Lohmann, U., & Leaitch, W. R. (2005). Importance of vertical velocity variations in the cloud droplet nucleation process of marine stratus clouds. *Journal of Geophysical Research*, *110*(D21), D21213. https://doi.org/10.1029/2004JD004922